

Testing the Re-designed SuperDARN HF Radar and Modeling of a Twin Terminated Folded Dipole Array

Kevin Tyler Sterne

Thesis submitted to the faculty of the Virginia Polytechnic Institute and State University
in partial fulfillment of the requirements for the degree of

Master of Science
In
Electrical Engineering

J. Michael Ruohoniemi, Co-Chair

Joseph B. H. Baker, Co-Chair

Steven W. Ellingson

William A. Davis

April 22, 2010

Blacksburg, Virginia

Keywords: SuperDARN, HF radar, radar electronics, antenna construction, method of moments, NEC2, twin terminated folded dipole

Testing the Re-designed SuperDARN HF Radar and Modeling of a Twin Terminated Folded Dipole Array

Kevin Tyler Sterne

ABSTRACT

The Super Dual Auroral Radar Network (SuperDARN) is an international collaboration of researchers interested in Earth's near-space plasma environment. This group uses high frequency (HF) radars and backscatter from magnetic field-aligned plasma irregularities to study space weather manifested in the Earth's magnetosphere and ionosphere. Space weather impacts many technological systems including Global Positioning System (GPS), spacecraft orbits, power distribution, surveillance radar, HF communications and transpolar aviation.

This thesis explores, in detail, the techniques and challenges of constructing, testing, and operating a newly designed SuperDARN HF radar. In modern times, the use of such frequencies for radar is limited to very specific applications and thus the topics presented are not common place. A new antenna design, the twin terminated folded dipole (TTFD), is analyzed along with the modeling results for several proposed and constructed phased arrays for this design. Finally, an initial radiation pattern measurement for the TTFD is presented and notes on how a similar measurement might be conducted on a TTFD phased array.

Acknowledgements

To begin, I would like to thank the many friends that have gotten me through almost a decade of my life and at times literally helping me back on my feet. It is these people that I have shared drinks with, explored the little quirks of life, and become who I am today. I also need to acknowledge my radio station family for their contributions in influencing my life. The people that I have met at WUVT have been some of my closest friends in the past few years at Virginia Tech.

I would also like to thank the members of my advisory board. I offer my thanks to Dr. Baker and Dr. Ruohoniemi for taking me aboard their research group and allowing input from graduate students, like myself, on their projects. I would also like to thank Dr. Davis and Dr. Ellingson for furthering my education throughout my undergraduate and graduate studies.

Thanks must also go to Dr. Greenwald for his initial work with the new antenna design found in this research. The advice and knowledge on the antenna as well as in several other areas laid the foundation and made it possible for me to complete this work.

Finally, I would like to thank members of my family for getting me through my younger years. First my mom, Suzanne Grimes, who always found a way to motivate me whether good or bad. Also, thanks goes to my dad, Randall Sterne, who always made time to welcome a visit no matter how busy I had been. John, Sheri, Timothy and my grandparents, the Grimms and the Grimes, thanks for being such a great and supportive family. A special thank you goes to my grandfather, Ronald Sterne, who never saw this work but always taught me how to enjoy life. And always, I live for 32. Thank you.

Table of Contents

1. Introduction	1
1.1. History of Ionospheric Radar	1
1.2. SuperDARN	8
1.3. SuperDARN Antennas	12
1.4. Thesis Organization	14
2. HF Radar Design and Operation	16
2.1. Introduction	16
2.2. Leicester Radar Electronics	18
2.2.1. Transmit Path	18
2.2.2. Receive Path	21
2.3. Receiver Front End	24
2.3.1. Design	24
2.3.2. Build	26
2.3.3. Tests and Results	28
2.4. Transmitter Test Setup	31
2.4.1. Design	32
2.4.2. Results	34
2.5. Antenna Array Construction	36
2.5.1. Guy Wire Support	39
2.5.2. Reflector Wire Construction	43
2.5.3. Antenna Construction	47
3. Modeling the TTFD Antenna Design	52
3.1. Introduction	52
3.2. The Numerical Electromagnetics Code (NEC) 2	55
3.2.1. Method of Moments	56
3.2.2. Approximations	58
3.2.3. Effect of Ground Plane	59
3.2.4. Modeling Physical Antenna Components	61

3.2.5.	Radiated Field Calculation	62
3.3.	EZNEC	63
3.4.	Previous Simulation of the TTFD Antenna	65
3.5.	Twin Terminated Folded Dipole – SuperDARN	67
3.5.1.	Modeling the Effect of an Antenna Splice	70
3.5.2.	The Hays Learning Experience	73
3.5.3.	Revisiting the Effect of an Antenna Splice	79
3.5.4.	Falkland Island Variations	80
3.5.5.	Full Array Modeling	88
4.	Conclusions and Future Work	92
	Appendix A: Wire Endpoints for Single TTFD in EZNEC for the Ideal Model	95
	Appendix B: Wire Endpoints for Single TTFD in EZNEC for the Implemented Model	96
	Appendix C: Results of a Previous Measurement of a TTFD Antenna	97
	List of References	102

List of Figures

Fig. 1.1 An ionosonde antenna in the foreground on Svalbard [2].....	2
Fig. 1.2 An example of an ionogram [3].....	3
Fig. 1.3 Description of single hop ground backscatter [4].....	5
Fig. 1.4 Seven-pulse transmission sequence used at the temporary radar site in 1982 [10]	9
Fig. 1.5 The Goose Bay HF radar site with the interferometer array pictured in the left background.....	10
Fig. 1.6 A common data product of SuperDARN radars operating in the northern hemisphere [16].....	11
Fig. 1.7 Twin terminated folded dipole antenna.....	13
Fig. 1.8 SuperDARN radar site at Blackstone, VA featuring the TTFD antenna design .	14
Fig. 2.1 Block diagram of general radar system.....	17
Fig. 2.2 The driver amplifier on the left and the pre-driver amplifier on the right.....	19
Fig. 2.3 Block diagram for the transmit path of the Blackstone HF radar.....	20
Fig. 2.4 A block diagram of the receive path for the Blackstone HF radar.....	22
Fig. 2.5 Block diagram of the receiver front end to be used at the Kapuskasing site.....	24
Fig. 2.6 The completed receiver front end board to be installed at the Kapuskasing radar site.....	27
Fig. 2.7 Gains and losses on system components of the receiver front end board.....	28
Fig. 2.8 Receiver board design with minor changes, addition of bandpass filters and changes to L.O. signal routing, as tested at Blackstone and installed at Kapuskasing	30
Fig. 2.9 Transmitters in the rack that will replace the Leicester transmitters at the Blackstone site.....	31
Fig. 2.10 Electrical schematic of pulse generator for transmitter test unit.....	33
Fig. 2.11 The completed transmitter test unit with an on/off switch and several SMA connections for RF and control signals.....	33
Fig. 2.12 Resulting waveforms for the transmitter test unit.....	35
Fig. 2.13 Process of building a SuperDARN antenna array.....	36

Fig. 2.14 A concrete pillar with threaded rods with an assembled pole ready to be raised and mounted on the pillar.....	37
Fig 2.15 Most of the antenna poles positioned with the guy wires temporarily tied into the ground anchors at the Hays site.....	38
Fig. 2.16 A side view of the guying and wire construction of the TTFD antenna array ..	40
Fig. 2.17 A front view of the guying and antenna wire construction of a TTFD antenna array. The hexagonal shape of the TTFD design can be seen in the middle of the figure.	41
Fig. 2.18 Installation of the horizontal cables with markings shown	42
Fig. 2.19 The installed horizontal guy wires as well as a resistor box.....	42
Fig. 2.20 Hog ring attachment to the guy cables using two sizes of hog rings.....	44
Fig. 2.21 The slanted bars at one end of the Hays radar with reflector wires attached	45
Fig. 2.22 Tangled or loose reflector wires along one section of the TTFD array at the Hays radar in Feb. 2010	47
Fig. 2.23 Dimensions of half of a TTFD antenna	48
Fig. 2.24 The middle antenna wire being attached to the balun on the right and secured to the horizontal guy on the left.....	49
Fig. 2.25 Coaxial cable entering the building from one radar and connectors being attached.....	51
Fig. 2.26 Sample radar data from the two Hays, Kansas radars	51
Fig. 3.1 The current expansion functions of a wire of four segments. The lower sinusoidal lines are summed to create the top sinusoidal line. [21]	57
Fig. 3.2 The summed current along a half wave dipole antenna with a center fed current source.	58
Fig. 3.3 The user interface for the EZNEC program	65
Fig. 3.4 TTFD antenna with reflector as modeled and tested at Saskatoon [20].....	66
Fig. 3.5 Vertical Slice of TTFD Pattern[20]	67
Fig. 3.6 Horizontal Slice of TTFD Pattern at an Elevation Angle of 30°[20]	67
Fig. 3.7 An array of 4 TTFD antennas similar to arrays at Blackstone	68
Fig. 3.8 An EZNEC model of the butt splice at Blackstone	69
Fig. 3.9 Preliminary SWR plot of TTFD antenna model without splice, the ideal model	71

Fig. 3.10 Preliminary SWR plot of TTFD antenna model with splice, the implemented model at Blackstone	71
Fig. 3.11 Measured SWR values for individual Blackstone antennas and the average Wallops antenna and for a modified model antenna	72
Fig. 3.12 SWR Measurements taken at Hays, KS with the Array Solutions baluns for selected poles.....	74
Fig. 3.13 SWR readings from a modified Array Solutions balun terminated into 2100 Ohms on the antenna side.....	77
Fig. 3.14 SWR measurements taken at Blackstone in order to field test the modified Array Solutions balun.....	78
Fig. 3.15 SWR Measurements for similar unmodified baluns mounted on TTFD antennas at Hays and at Blackstone	78
Fig. 3.16 SWR of the ideal antenna model without a splice and with higher standardizing impedance, Z_0	79
Fig. 3.17 SWR of implemented antenna model with a splice and higher standardizing impedance, Z_0	79
Fig 3.18 Different antenna orientations used to investigate the Falkland Island setup. The bar shows how the horizontal axis for each antenna is manipulated for each variation.....	81
Fig. 3.19 Radiation pattern for 8 log-periodic antennas in a regular orientation.....	82
Fig. 3.20 Radiation pattern for 8 log-periodic antennas in a tilted orientation.....	82
Fig. 3.21 Azimuth plot of radiation pattern for a regular half array of TTFDs	84
Fig. 3.22 SWR plot for a regular half array of TTFDs	84
Fig. 3.23 Azimuth plot of radiation pattern for a half array of slanted TTFDs	85
Fig. 3.24 SWR plot for a half array of slanted TTFDs	85
Fig. 3.25 Azimuth plot of radiation pattern for a half array of tilted TTFDs	86
Fig. 3.26 SWR plot for a half array of tilted TTFDs	86
Fig. 3.27 The Falkland Island SuperDARN radar site with newly installed log periodic antennas (Feb. 2010).....	87
Fig. 3.28 Azimuth pattern at max gain elevation angle for TTFD array at 14 MHz	88

Fig. 3.29 Azimuth pattern at max gain elevation angle for log-periodic array at 14 MHz	88
Fig. 3.30 The elevation pattern of an array of TTFD antennas at 10 MHz.....	90
Fig. 3.31 The elevation pattern of an array of TTFD antennas at 14 MHz.....	90
Fig. 3.32 Azimuth pattern of a full TTFD array steered to one extreme of the array's scan at 14 MHz.....	91
Fig. 3.33 Azimuth pattern of a full TTFD array steered to one extreme of the array's scan at 18 MHz.....	91
Fig. C.1 TTFD construction at Saskatoon [20].....	97
Fig. C.2 Measurement Setup performed at Saskatoon.....	98
Fig. C.3 Radiation pattern plots from the measurements taken at Saskatoon of the prototype TTFD antenna with the dashed lines representing 5dB [20]	100

List of Tables

Table 1.1 Condensed history of radio and use of radar for ionospheric studies up until the 1980s.....	8
Table 2.1 General SuperDARN radar transmission and control signal characteristics....	32
Table 3.1 Antenna models created and analyzed with EZNEC.....	64
Table 3.2 Local factors impacting antenna array performance	73

1. Introduction

1.1. History of Ionospheric Radar

In the late 1800s several scientists were developing methods of creating wireless telegraphy technology. Among them Heinrich Rudolf Hertz used Maxwell's theory of electromagnetism to predict the transmission and reception of electromagnetic waves in an experiment conducted with prototype antennas. Wireless telegraphy and radio as a communications tool were further developed and popularized by Guglielmo Marconi at the turn of the 20th century. Most notable was Marconi's claim in December 1901 that he had received the Morse code letter 'S' on a transatlantic link comprised of a transmitting station in England and a receiver in Newfoundland. A couple of months later in February 1902, Marconi conducted a more scientific experiment by recording signals received on board a ship sailing away from the same transmitting station in England. During this experiment, Marconi noticed that he received signals at night about 2,000 miles away from the transmitting station, whereas during the day the signals were received only as far as 700 miles. This experiment sparked theories about how radio signals were received at such large and varying distances.

The same year as Marconi's ship experiment, Arthur Kennelly and Oliver Heaviside independently predicted that a layer of ionized gas allowed radio waves to

travel beyond the horizon. This layer of the ionosphere, originally known as the Kennelly-Heaviside layer, was not proved to exist until experiments in 1924 by Edward Appleton and in 1925 by Gregory Breit and Merle Tuve [1]. Appleton was able to use a British Broadcasting Corporation transmitter and regularly change the frequency of transmission. With change in frequency, Appleton measured the time it took the signal to travel to the ionosphere and back to the ground.

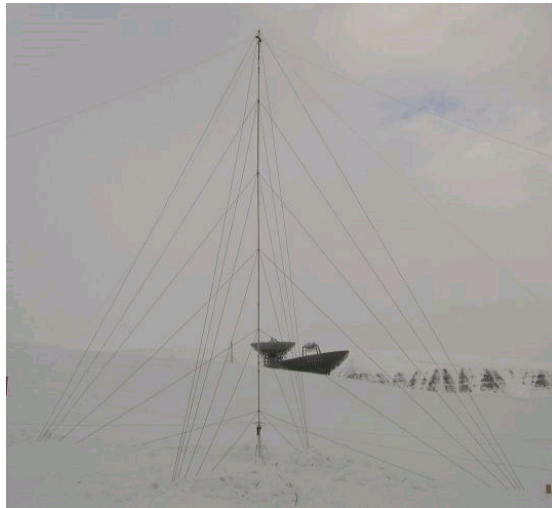


Fig. 1.1 An ionosonde antenna in the foreground on Svalbard [2]

Similarly, Breit and Tuve used developing radar technology to create an ionosonde. A modern version of an ionosonde antenna is pictured in Figure 1.1. This special type of radar uses a single pulse of radio frequency (RF) energy sent vertically and receives the signal bounced back from the ionosphere. Measuring the time between the transmitted signal and the received signal yields the height at which the signal bounces back. Breit and Tuve found that by varying the frequency of the RF in the transmitted pulse, the echo height of the returned signal varied. This system used high frequencies (HF) in the range of 3 to 30 MHz since numerous communications systems had been developed using this part of the frequency spectrum. These communication

systems had gained popularity because of the propagation characteristics demonstrated in the experiments by Marconi.

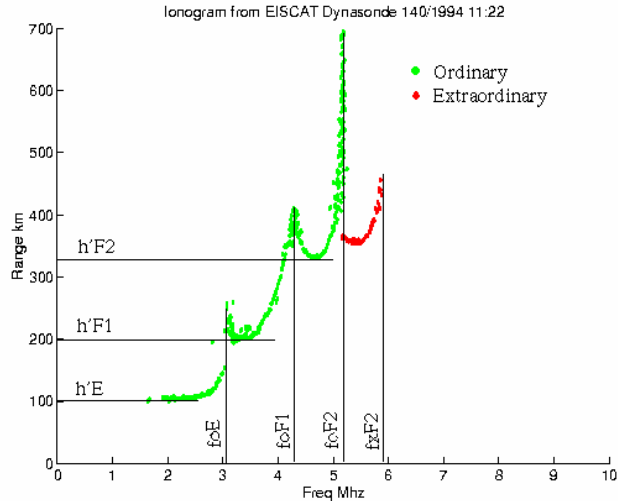


Fig. 1.2 An example of an ionogram [3]

Breit and Tuve's experiment on the height of returned signals led to the invention of ionograms (Figure 1.2). The ionogram shows the transmitting frequency along the horizontal axis and the height according to the propagation delay of the returned signal along the vertical axis. Scatter for a given frequency occurs at the height where the transmitted frequency equals the local plasma frequency, partially determined by the density of the ionosphere layer. The relation of the plasma frequency, ω_{pe} , to the plasma density is given by:

$$\omega_{pe} = \sqrt{\frac{n_e e^2}{m^* \epsilon_0}}$$

where n_e is the number density of electrons, e is the electric charge, m^* is the effective mass of the electron, and ϵ_0 is the permittivity of free space. The variables in this relationship are the frequency, ω_{pe} and the density of electrons, n_e ; so as the density of

electrons in the ionosphere increases, the frequency which is reflected increases. This frequency matching constitutes critical reflection. As the frequency is increased, the height of the echo return generally increases because the density of the ionosphere increases with height. The upper frequency limit of the ionogram varies depending on the plasma frequency of the densest layer of the ionosphere. Higher frequencies penetrate the densest layer and less dense layers above this point will not scatter the signal back to the ground. The lower frequency limit to an ionogram is defined by the absorption of frequencies lower than about 2 MHz in the lower ionosphere. An ionogram identifies distinct layers in the ionosphere noted in Figure 1.2 as E, F1, F2; the notation of h' shows the height of each layer and the f_o notation shows the plasma frequency for that layer. The layers are created mostly by photochemical and transport processes in the Earth's upper atmosphere.

Before radar technology was used to understand the ionosphere, radar-like technology was developed for much simpler purposes. In 1904, Christian Huelsmeyer developed a separated transmitter and receiver system that allowed a ship to detect if another ship was close by. This primitive radar did not give any range information but was useful in times of heavy fog. It was not until the 1920s and 1930s that radar technology was developed for scientific purposes. Breit and Tuve's work in developing a system that allowed for the transmission of a pulsed RF signal and measurement of the range of the echo sources became one of the foundations of radar technology.

Radar was further developed as an early warning detection for ships and aircraft in the build-up to World War II. Because of the need for secrecy, radar was developed independently in several different countries. Several long distance radar systems had

trouble with interference caused by mysterious, stationary backscatter sources at frequencies above the expected maximum critical frequency of the ionosphere. In a post-war publication in 1951, W. G. Abel and L. C. Edwards [4] noted that several teams of researchers had developed their own theories about the sources. Abel and Edwards were able to determine that most of the stationary backscatter observed on their long distance radar system was the result of a single reflection off the ionosphere followed by backscattering from the Earth's surface as seen in Figure 1.3.

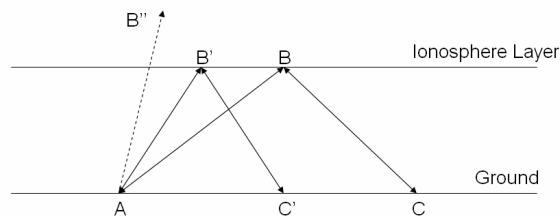


Fig. 1.3 Description of single hop ground backscatter [4]

For frequencies that are transmitted somewhat above the maximum critical frequency, or trans-critical frequencies, for vertical incidence, the radio wave will follow a path similar to ABC in the figure in what is called oblique incidence. Roughness of the ground will backscatter some of the signal to point A. As the elevation angle increases the ionosphere continues to reflect signals off the ionosphere until an angle is reached for which the transmission penetrates the ionosphere, as in the case of AB'' . This limit is defined by the path of $AB'C'$ and as a result ground reflection can occur over a wide area. This type of backscatter was unwanted by early warning radar operators, but became an interesting tool for researchers interested in HF propagation modes.

In the years following Abel and Edwards' study, researchers determined that under some conditions the ionosphere backscattered trans-critical signals directly to the radar instead of simply bouncing signals from the ground. In 1960, H. F. Bates [5]

experimented with radio wave propagation by using an HF radar to measure ground backscatter. From his studies, Bates regularly observed two modes of direct scatter from the arctic F region of the ionosphere:

1. Backscatter from randomly distributed, field-aligned irregularities, primarily observed during nighttime
2. Backscatter from the field-aligned boundary of irregularly ionized patches that are relatively thin perpendicular to the geomagnetic latitude lines, primarily observed during daytime

Radars studying the ionosphere received backscatter from irregularities that are aligned with the Earth's magnetic field. In order to reflect a signal off the irregularities, the signal needs to travel in a direction orthogonal to the geomagnetic field lines. This condition limits observing field-aligned backscatter to certain locations on the Earth. Two areas where radars can easily send a radio wave orthogonal to the geomagnetic field lines are in the high-latitude and equatorial zones and thus radars conducting ionospheric studies are often located in these regions.

Two years before Bates' experiment, W. E. Gordon theorized that a high power incoherent scatter radar could reflect signals off free electrons with a vertical incidence radar and measure electron densities and temperatures in the ionosphere [6]. Bowles demonstrated Gordon's theory the same year in 1958 with a pulsed radar system that had a peak pulse power of 4 to 6 MW and measured electron densities in lower levels of the ionosphere [7]. The high power output was required since the cross section of a single electron is relatively small and thus the reflected signal level is very low. Powerful radars were subsequently developed to exploit the radar returns from free electrons,

which constitutes incoherent scatter; however, the focus of SuperDARN and this thesis deals more with radar signals reflected off plasma density irregularities which constitutes coherent scatter.

One study using radars to reflect signals off irregularities in the ionosphere was conducted in Alaska [8]. Two VHF coherent radars with narrow fixed beams measured backscatter signals from irregularities and observed Doppler shift from the drift velocities of the irregularities. Since these irregularities are field-aligned, their motion indicates the drift of plasma in the plane perpendicular to the magnetic field, which at high latitudes is almost horizontal. The motion observed is a component of the $\vec{E} \times \vec{B}$ drift resulting from an ionospheric electric field, \vec{E} , with $\vec{v} = \frac{\vec{E} \times \vec{B}}{B^2}$. The two Alaskan radars were separated in azimuth by about 45 degrees allowing for a common measured volume of about 800 km². A few years after this experiment, a new pair of radars, constructed in Scandinavia, used a phased array of antennas to create several beams and achieve a common volume area of about 230,000 km². This system became known as the STARE (Scandinavian Twin Auroral Radar Experiment) radars and also used VHF frequencies to bounce signals from field aligned irregularities in the ionosphere. The STARE radars measured Doppler velocities of the returned signals which were presented in [9]. The results of these two radar experiments led researchers to further improve upon their radar designs to study field aligned irregularities in the ionosphere and to understand motions in space plasma.

Table 1.1 below can be used as a quick reference for the history presented so far in the development of radar and its use in ionospheric study.

Year	Event
1886-1888	- Hertz uses Maxwell's equations to predict the transmission and reception of electromagnetic waves
1901	- Marconi claims to receive the first transatlantic wireless telegraphy signal
1902	- Marconi repeats the experiment aboard a ship in the Atlantic and notices farther signal reception at night than during the day
1902	- Kennelly and Heaviside predict ionized gas layer
1904	-Huelsmeyer develops a radio system for ships to detect the presence of other ships.
1924	- Appleton develops a system measuring the height of radio wave reflections off the ionosphere
1925	- Breit and Tuve developed pulsed transmission system for measuring the height of the ionosphere reflected signals, develop ionosonde
Late 1920s & 1930s	- Several countries independently developed early warning aircraft and ship detection systems through the use of radar
1951	- Abel and Edwards determined the source of long range backscatter is from signal bouncing off the ground
1958	- Gordon theorized use of high power radar signals to observe free electrons in the ionosphere
1958	- Bowles observed free electrons as theorized by Gordon
1960	- Bates published results of returns from an HF radar and notes that the returns are from field aligned irregularities in the ionosphere
1971	- Ecklund, Balsley, and Greenwald experimented with coherent VHF radar systems with a common volume to determine vector components of irregularity drift velocity
1977	- Greenwald, Weiss, and Nielsen completed STARE radars; larger common volume with two radars, used coherent radars

Table 1.1 Condensed history of radio and use of radar for ionospheric studies up until the 1980s

1.2. SuperDARN

After the published results of the STARE radars, researchers wanted to expand the field of view of the radars as well as improve their techniques for measuring parameters from radar returns. One of the next radars to study the ionosphere was temporary installation near Fairbanks, Alaska and used HF for its pulsed RF transmission. HF allows for backscatter from longer propagation distances because

ionospheric refraction can bend the signal to propagate nearly horizontally. Results for this temporary radar were published by Greenwald, et al, in 1983 [10]. This radar system used a seven-pulse transmission sequence in order to identify range information of multiple returns as well as to increase the Doppler velocity resolution. Since the transmitted pulse sequence was known, the received pulse sequences were identified by comparing them to the transmitted sequence. This comparison allowed the receiver to separate received pulses from multiple ranges even if the sequences overlap. As seen in Figure 1.4, the pulse sequence is designed such that several multiples of a common time spacing, t_0 , are created. Each multiple of t_0 is known as a lag and so in the pulse sequence below, there are 16 lags. Since t_0 is known, the Doppler velocity can be found from the received pulses by measuring the phase variation with lag. The results from this radar operation were limited due to inadequate antenna arrays to accomplish the desired beams.

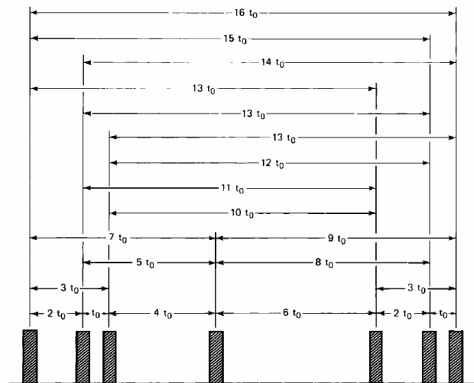


Fig. 1.4 Seven-pulse transmission sequence used at the temporary radar site in 1982 [10]

With the results of the test of the HF radar system in Alaska [10], an HF radar was constructed in Goose Bay, Labrador in 1983. This radar successfully received backscatter from decameter-scale irregularities in the ionosphere while operating on a daily basis [11]. The radar at Goose Bay was also able to record Doppler velocity through

the use of a multi-pulse transmission sequence. The radar used 16 horizontal log-periodic antennas for its main transmitting and receiving array. In 1987, an additional array of the same log-periodic antennas was added in front of the main array as pictured in Figure 1.5 in order to provide elevation data through interferometry [12]. This setup of the main array and interferometer arrays was duplicated at several new radar sites around the auroral zone.

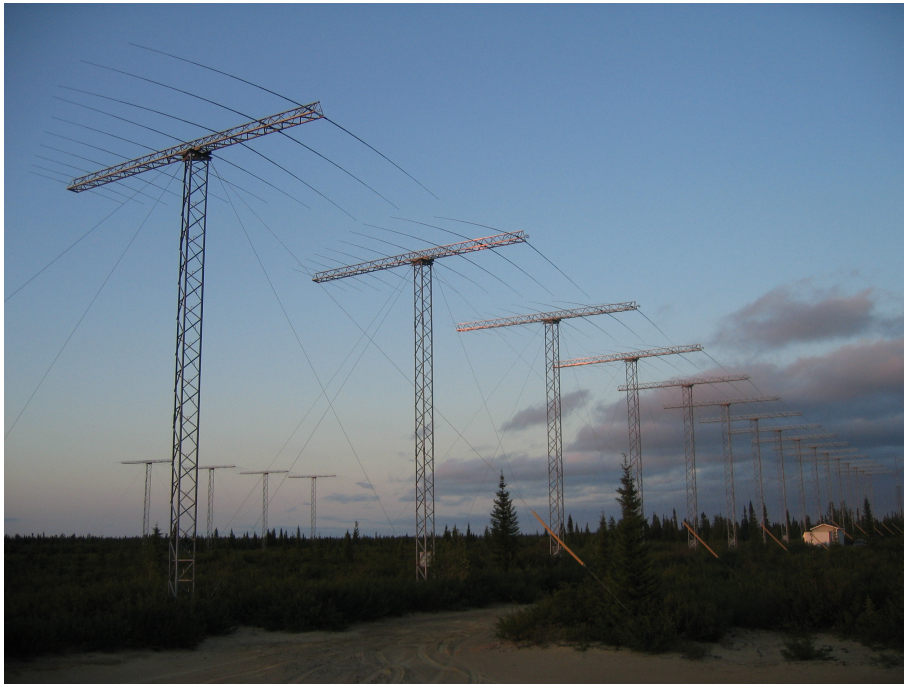


Fig. 1.5 The Goose Bay HF radar site with the interferometer array pictured in the left background

Eventually, the Goose Bay radar and the other auroral radars were grouped together to become known as the Super Dual Auroral Radar Network (SuperDARN). The SuperDARN radars are constructed and maintained by several research groups in an international collaboration in space weather research [13]. SuperDARN also encompasses the southern hemisphere so that both magnetic poles can be monitored simultaneously [14]. Each radar produces the same data product such that at any given

time, data from every radar can be easily compiled together and a snapshot of the ionospheric conditions provided. One data product for the SuperDARN group is the drift velocity and position of returns from field aligned irregularities in the ionosphere. These measurements from multiple radars can be used to produce a space weather map of ionospheric plasma motion [15]. An example of this map can be seen in Figure 1.6. In this figure, the drift velocity direction is marked by the direction in which the line extends from each dot. The magnitude of the drift velocity is marked by the length of this line as well as by color. The pie-shaped field-of-views of the SuperDARN radars can be seen in this figure.

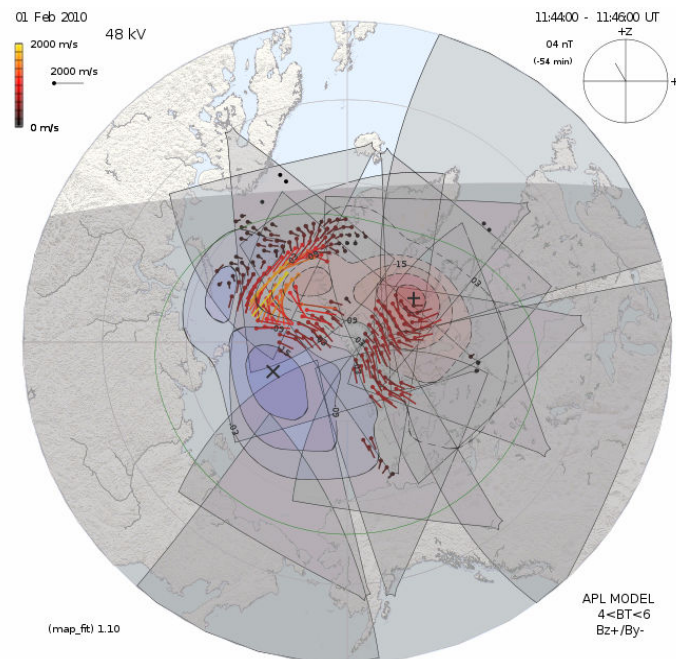


Fig. 1.6 A common data product of SuperDARN radars operating in the northern hemisphere [16]

This figure uses sun-fixed coordinates with the magnetic pole at the center of the figure and the sun to the top of the figure. The figure also shows the electrostatic potential contours inferred from the velocity measurements. This map of space weather conditions

is used by researchers in order to understand other ground-based and spacecraft measurements relating to the ionosphere and the Earth's space weather.

1.3. SuperDARN Antennas

At the Goose Bay radar, the log-periodic antennas were designed and constructed by the Sabre Communications Corporation in Sioux City, Iowa and measured close to 50 feet wide and close to 40 feet long. Log-periodic antennas are known to create a very directional beam and asymmetric radiation pattern which are needed for the HF radars. Using many of these antennas in a phased array allowed for a narrow, steerable beam. In order to support such a large antenna, significant towers needed to be built. Over time, the cost of constructing the antenna arrays became a significant part of the overall cost of building a new radar. In order to reduce the cost of building a new radar, the SuperDARN researchers needed a cheaper antenna design.

The twin terminated folded dipole (TTFD) was introduced as a replacement to the Sabre design during the construction of lower latitude radars [17]. This new design was created by SuperDARN's Ray Greenwald in the early 2000s. Greenwald drew his inspiration from the Barker and Williamson antenna design [18] which uses a single folded dipole but the two folded-dipole concept came from Kraus' antenna book [19]. The TTFD antenna design, seen in Figure 1.7, uses very few wires and at 8 feet high and 36 feet wide, is relatively small in size compared to the log-periodic design. The feed point of the antenna consists of a 25:1 balun located at the center of the middle horizontal wire and its location is represented as a gray box in Figure 1.7. The white squares on the

top and horizontal wires in the figure represent resistive loads. The RF coaxial line is fed up a pole located at the center of the antenna.

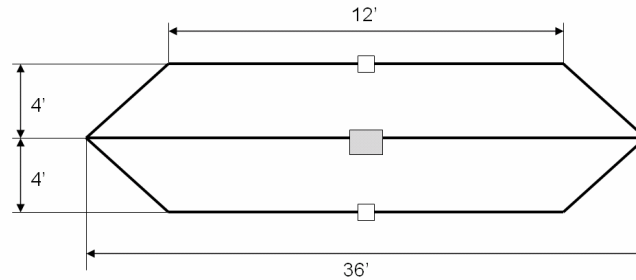


Fig. 1.7 Twin terminated folded dipole antenna

Constructing the supporting structure for this antenna design is also simplified from the Sabre design by using vertical poles and running Kevlar cable horizontally between the poles as supports. Then the conducting wire is attached to the Kevlar cables to form the hexagonal shape of the TTFD design. Since the TTFD design is not very directional by itself, a corner reflector is added to the rear of the antenna array. In the most recent design the reflector is constructed by running 21 conductive wires horizontally along the length of the array. The spacing between the wires, approximately 1 meter, is small enough compared to the radar wavelengths, 17 to 35 meters, that the wires act like a solid surface reflecting the power incident on the reflector wires into the forward direction.

As with the Sabre design, sixteen of the TTFD antennas make up the front array and an additional four make up the interferometer array. The TTFD antenna has already been deployed at radar locations at Wallops Island (2005) and Blackstone, Virginia (2008), pictured in Figure 1.8, as well as at newly constructed sites in Hays, Kansas (2009) and near the McMurdo Station in Antarctica (2010). However, the radiation pattern of these arrays has yet to be fully analyzed.



Fig. 1.8 SuperDARN radar site at Blackstone, VA featuring the TTFD antenna design

1.4. Thesis Organization

It is the purpose of this work to analyze, in detail, the performance of the HF radar used for ionospheric research by the SuperDARN research group at Virginia Tech. This detail will include analysis of the electronics designed by the University of Leicester and temporarily installed at Blackstone, Virginia in the second chapter. This chapter will also show analysis of a receiver front end recently installed in a radar site in Kapuskasing, Ontario; the design of a transmitter test setup; and the construction techniques of new SuperDARN radars in Hays, Kansas. In the third chapter, the TTFD antenna design will be modeled and the radiation pattern analyzed as it is used at several radars. This chapter will also feature a discussion of the software used to model the antenna array called EZNEC Pro v. 5.0. This software is based on the Numerical Electromagnetics Code

(NEC) 2 algorithm and a discussion of code's history and development will be presented in the third chapter. This discussion of NEC2 and EZNEC is presented in the third chapter to provide background for the modeling techniques used in this work. Previous modeling for a prototype TTFD antenna design is also presented in the third chapter. Modeling results for this work are then presented which include a few variations on the original TTFD design.

In the fourth and final chapter of this work, conclusions and ideas for further work on the topics are presented.

2. HF Radar Design and Operation

2.1. Introduction

The basic idea for a radar system is to provide range and direction information by the use of radio signals. Range information can be gathered since the speed of a radio signal is known and the time the signal takes to return after being transmitted can be measured. Direction information is usually gathered from the direction of a directional antenna's main radiation beam. A simple system overview of radar and some basic components can be seen in Figure 2.1. The radar process starts in the RF pulse generator in which an RF pulse sequence is generated. If the antenna is too large to be mechanically steerable, as is the case with SuperDARN, a phased antenna array is used to steer the main radiated beam. For a phased array, the RF pulse signals are split into the required number of signals and passed through a phasing matrix which applies a phase stagger to the signals in order to form the desired beam direction. This low power phasing of signals is performed in SuperDARN radars but does not necessarily occur for all phased array systems. Next, the RF pulses are directed to individual transmitters for each antenna and amplified up to the desired power level. One of the most critical parts of the radar system is the Transmit/Receive (T/R) switch in the transmitter that isolates the amplifier output from the receiver front end. This switch protects the sensitive

receiver front end from the high power signals coming out of the amplifier. The switch also allows for the system to use the same antenna for transmit and receive, saving on space and usually on cost. The radiated signal from the antenna is propagated into space and will scatter off objects. Some of the scattered signal is radiated back to the antenna where the signal then follows the receive path of the radar.

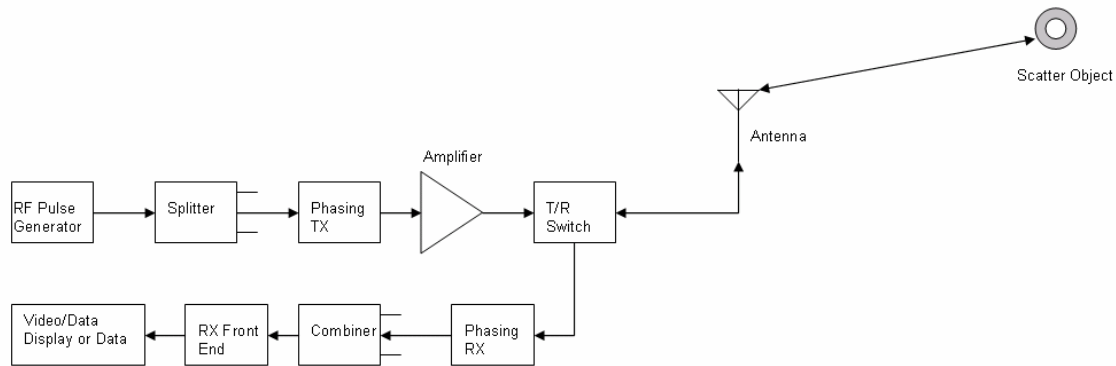


Fig. 2.1 Block diagram of general radar system

Once the RF signal is received, it is passed to the receiver electronics through the T/R switch. From the T/R switch, the received signal passes through another phasing matrix which applies a phase stagger on the signals like that formed on transmit. From here, the received RF signal passes to the receiver front end. The front end selects the desired RF signal and amplifies it for data processing. Here, the signal can either be displayed to convey information to a human user or stored digitally for later analysis.

A radar system is designed so desired objects are “seen” by the radar within certain parameters. A simplified version of the equation commonly used in radar system design is:

$$P_r = \frac{P_t G^2 \lambda^2 \sigma F}{(4\pi)^3 R^4}$$

where P_t is the power transmitted; G is the gain of the antenna, here it is assumed that the transmitting and receiving antenna are the same; λ is the wavelength of the transmitted frequency; σ is the radar cross section of the scattering object; R is the one-way range to the object; and F is a propagation factor that includes signal fading and other path losses. The radar cross section of an object depends on its reflectivity, the relative size of the object to the wavelength of the RF pulse and the angle of incidence on the object. Variables in this equation are manipulated so that the power received, P_r , is above the noise power enough that the receiver can detect the scattered signal. The required signal-to-noise ratio varies from system to system.

In order to monitor the motion of plasma in the ionosphere, SuperDARN uses high frequency (HF) radars which are equipped to monitor the Doppler shifts imparted to a signal that is backscattered from electron density irregularities that are drifting with the ambient plasma. While there are several versions of the SuperDARN radar electronics, the next section examines from a system perspective how the radar at Blackstone, Virginia, functions. As the title of this section indicates, the electronics at Blackstone were provided by the University of Leicester in the United Kingdom.

2.2. Leicester Radar Electronics

2.2.1. Transmit Path

The multi-pulse sequence mentioned earlier is generated through coding in a computer called the DDS Box. From there the signal passes through the first of many

T/R switches. Next, the pulse sequence is formed into 16 time delayed signals in order to form the desired beam direction. The time delay of each of the signals is generated in the phasing matrix. Next, the signals are sent to a combiner and if stereoscan is enabled, the signal is combined with the other channel. Stereoscan is a special type of scan introduced in the Blackstone radar in which the radar generates signals at two different frequencies and beam directions. If each of the different frequencies is to be transmitted on a different beam, then the radar requires that each frequency use its own phasing matrix. The two phasing matrices are present at the Blackstone radar. The combiner unit acts as a splitter on the receive side and will be mentioned in the receive path description.

From the combiner/splitter, the signals enter their respective transmitter at roughly 0 dBm. The first part of the transmitter is a low power T/R switch which allows the received signal to bypass the amplifier chain. The low power T/R switch also contains a high pass filter to clean up the signal coming from or going to the phasing matrix. Next, the signal is amplified up to the desired power output.

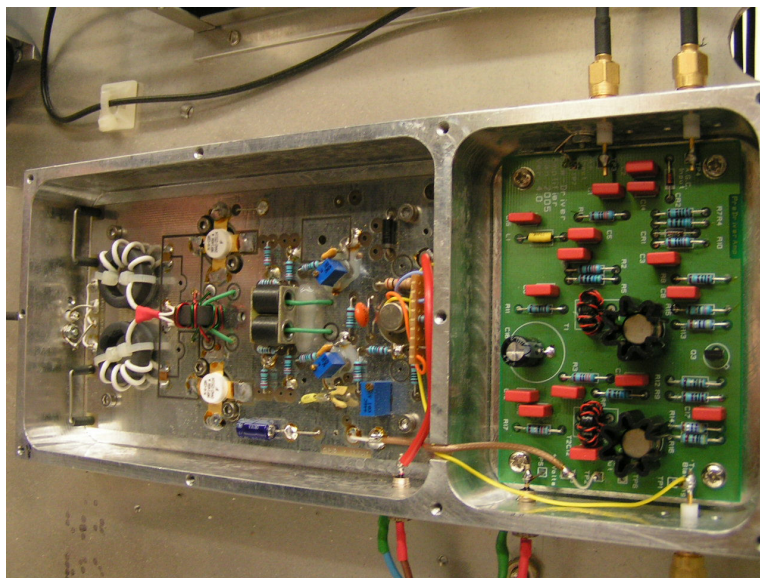


Fig. 2.2 The driver amplifier on the left and the pre-driver amplifier on the right

The first stage, the pre-driver amplifier, sets the final output level as it is a variable gain amplifier with a range from 0 to 26 dB. After the first stage, the driver amplifier and the final amplifier boost the signal to the final power output. A picture of the circuit board for the driver amplifier and the pre-driver amplifier is presented in Figure 2.2. As seen in the block diagram in Figure 2.3, the maximum gain of the transmitter is about 64 dB. Put into terms of power, this amount of gain means that 0 dBm input to the pre-driver amplifier will be amplified up to around 2.5 kW at the transmitter output. However, because of potential distortions of the signal levels above 800 Watts, the transmitters at Blackstone are typically set to output 500-600 Watts peak power. The duty cycle of the RF pulses transmitted is typically 3% and so the average power is much lower than the peak power.

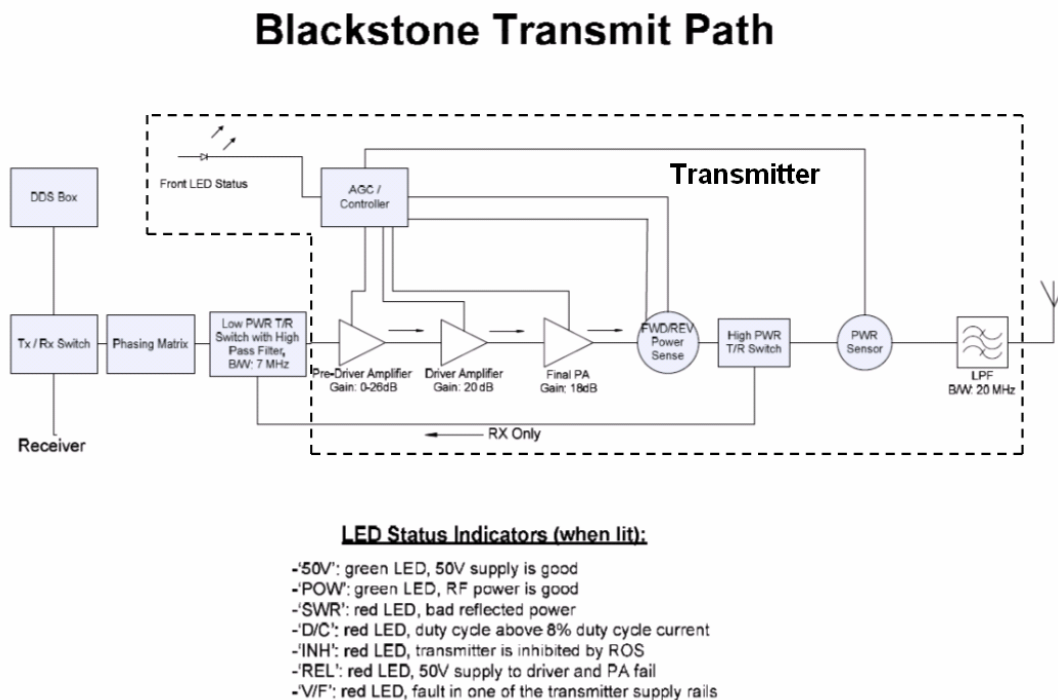


Fig. 2.3 Block diagram for the transmit path of the Blackstone HF radar

From the final amplifier, the signal passes through a forward and reverse power sensor. This sensor is designed to sense forward power as it is transmitted toward the antenna to ensure the amplifier units are operating properly. The sensor also senses the reverse power in order to detect conditions in which the amplifier should be shut down. One such condition is a problem with the input impedance of the coaxial cable connecting the transmitter to the antenna. This problem causes RF power to be reflected back into the transmitter which can potentially damage the transmitter's electronics. After this sensor, the signal passes through the final T/R switch and through another power sensor. The second power sensor in combination with the first power sensor can signal the controller unit if there has been a failure of the high power T/R switch. In the case of this switch failing, the controller senses forward power being transmitted before the switch, but does not sense any power after the switch. Finally, each of the signals passes through a low pass filter to ensure higher harmonics are not radiated out of the antennas.

The controller unit also drives several other status lights that are indicated in Figure 2.3. These provide for quick diagnostics of problems in the transmitter. A few of the status lights also work with the remote monitoring program so that the status of transmitters in remote locations can be monitored.

2.2.2. Receive Path

Once the signal is received on the antenna, the signal passes back through the transmitter on the receive path as indicated in Figure 2.4. Once the signal leaves the transmitter, the signal is split into two channels as described before for stereoscan. Each channel's receiver is identical except for the local oscillator frequency. From the splitter,

the signal goes back through the phasing matrix in order to form up the receiving antenna beam. From here, the 16 signals are combined into one signal through a 16-to-1 combiner. After being summed, the signal passes through a T/R switch which switches between the final parts of the receiver and the DDS Box.

The signal then passes through a three-part modular section of the receiver that is made up of a mixer, a filter bank, and an amplifier. The mixer includes a pre-amplifier to overcome some losses in the mixer and other parts of the receiver. The output of the mixer is an intermediate frequency (IF) of 40.625 MHz.

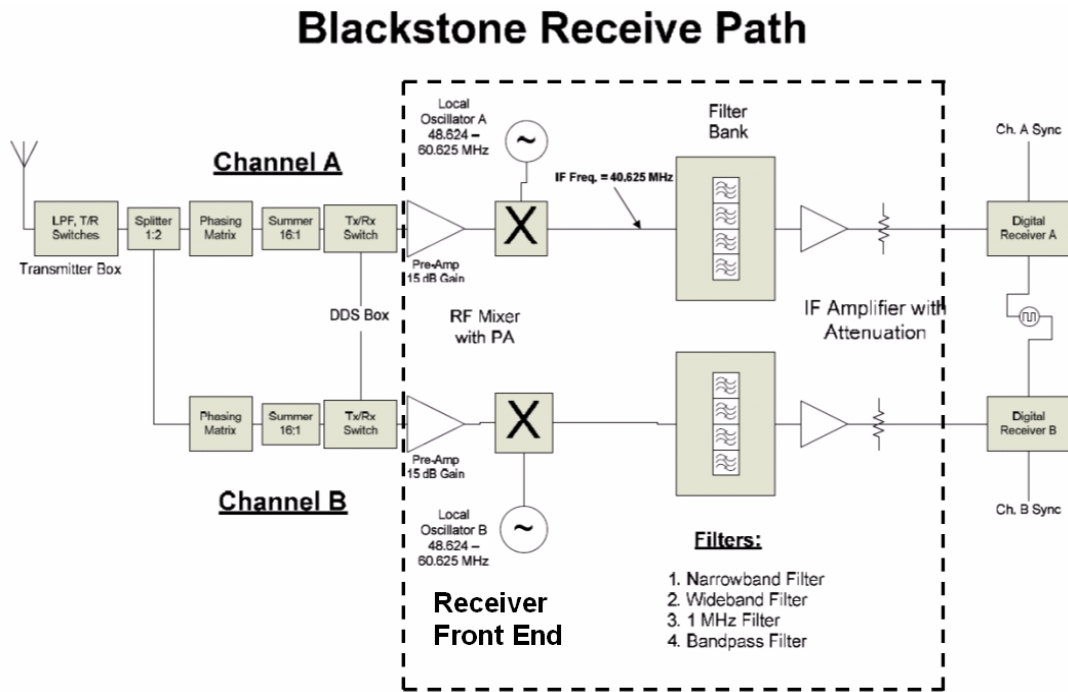


Fig. 2.4 A block diagram of the receive path for the Blackstone HF radar

From the mixer, the signal then passes through a filter bank, as seen in Figure 2.4, to eliminate unwanted mixing products. The filter bank has multiple filters since the electronics for this receiver are also used for applications other than SuperDARN radars. The narrowband and wideband filter have a bandwidth of 7 kHz and 20 kHz respectively.

These bandwidths correspond to using a 100 microsecond and a 300 microsecond pulse width. The 1 MHz filter is used for the pulse sequence that SuperDARN radars employ. The last filter noted on the figure is a 9-pole bandpass filter.

Lastly, before the signal passes to the receiver it passes through another stage of amplification in the IF amplifier. However, depending on the kind of application of the electronics, some attenuation may need to be added. The attenuator can be stepped from 0 dB to 70 dB in intervals of 10 dB. From there, the signal enters the digitizing receiver in which the signal is processed digitally, information is extracted and saved to a hard disk.

A similar receive path exists for the interferometer array at the SuperDARN radar at Blackstone which provides elevation angle information. However, in the interferometer array, the signal does not pass through a transmitter since the interferometer array does not transmit. To compensate for this difference in phase length, the signal passes through a phase shifter. If all the other cables connecting the various parts of the system are the same length then the signal from the main array and the signal from the interferometer array will arrive at the receiver at the same relative phase except for the phase difference introduced by the location difference. Since the front array and interferometer array are separated by a couple hundred feet, the interferometer signal will lag behind the main array signal. The amount of phase difference can then provide elevation angle information.

The Leicester electronics installed at the Blackstone radar are due to be replaced by our own electronics developed at Virginia Tech. The testing and development of some of the Virginia Tech electronics is presented in the next sections.

2.3. Receiver Front End

In this section, we will take a closer look at a receiver front end that was originally designed by Ray Greenwald and built and tested by myself. This receiver front end is to be installed at Kapuskasing and establishes the standard for receivers at existing and new radars. This section will feature a discussion of the design, the additional design and parts needed to build the receiver design, and tests of the performance of the receiver front end. This receiver front end was installed at the SuperDARN radar in Kapuskasing, Ontario in March 2010 along with a new digital receiver card.

2.3.1. Design

The receiver front end is designed to take the RF signals coming in from the antennas and up-convert them to a frequency that a digitizing card in a computer can read. The block diagram of the design of the board can be seen in Figure 2.5.

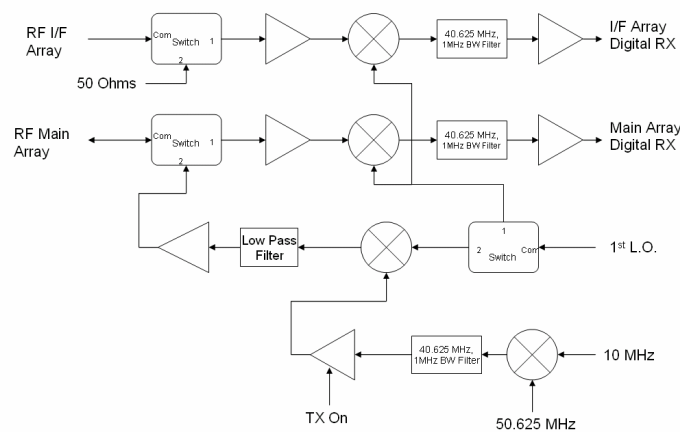


Fig. 2.5 Block diagram of the receiver front end to be used at the Kapuskasing site

The RF signals from the main and interferometer arrays enter the board after passing through the 16-to-1 combiner. The first switch is driven by a T/R signal which for the main array switches between signals being received and signals that are to be transmitted. From this input switch, the received signals are amplified and then mixed. The other input to the mixer is the first local oscillator (LO) which is set in order to have the desired IF of 40.625 MHz. In order to up-convert an RF signal in the range of 8-18 MHz to the IF frequency, the LO must be set for high side injection in the range of 48.625-60.625 MHz. For this design, the difference frequency between the LO and the RF signal is the desired signal out of the mixer. The first LO signal is switched between the receive side mixers and another mixer that will be covered later. The IF signal is then filtered through a 1 MHz wide bandpass filter centered on 40.625 MHz. The 1 MHz bandwidth is chosen so that Doppler frequency shifts of the backscattered signals can be analyzed without allowing undesired signals through. From the filtering, the signal passes through more amplification before it is passed to the digitizing card in a computer. From there, the digital samples are processed and stored in the computer.

The misnomer about this board is that it is not only a receiver front end, but also acts as the RF pulse generator for the radar. The pulse sequences are generated outside of this board, but the board takes the pulse sequence and creates RF pulses. The RF pulses are accomplished in the bottom part of the block diagram in Figure 2.5. The 50.625 and 10 MHz signals in the bottom right corner of the block diagram are references that synchronize this board with other parts of the radar. Here, they generate the required IF frequency that is then filtered and run through a variable gain amplifier. This amplifier turns the constant sine wave IF signal into the desired pulse sequence by turning on and

off the amplifier. Here, the pulse sequence input signal is labeled as 'TX On'. After the pulsed RF is created it is put into one input of the mixer. Now returning to the first LO switch, on the transmit side of the T/R signal, the switch passes the LO frequency out of port 2 to the mixer on the block diagram. The mixing between the first LO and the pulsed IF creates the desired RF frequency. After passing through a low pass filter to eliminate other mixing products the signal is then amplified to overcome the mixing and filter losses. The pulsed RF signal then passes to the T/R switch at which it will be in the transmit mode and pass the RF signal to the 16:1 combiner/splitter and then to the transmitters.

2.3.2. Build

In taking the receiver board design and implementing it to function at the radar site, a few additional design items were needed. All of the components of the block diagram, except for the filters, were translated into Mini-Circuits components and connected together through coaxial cables. However, all of the amplifier and switching components needed to be powered by either a 15 Volt (V) source or a +/- 5 V source. From this, two DC power supplies were added to the board and their DC outputs wired to a terminal block such that multiple components could also be wired to the terminal block. The 120 VAC input to these power supplies was fused to protect the electrical components and run through a switch to control the power to the board.

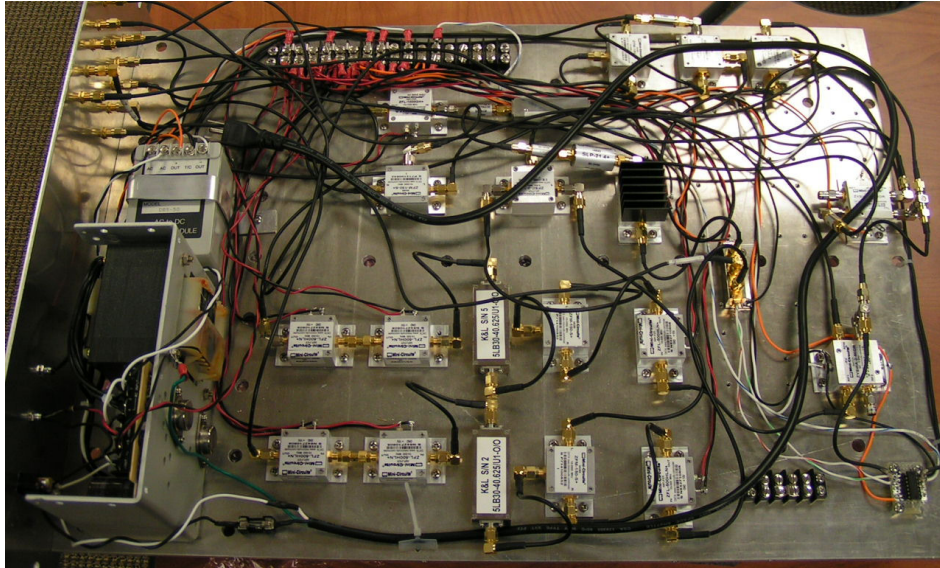


Fig. 2.6 The completed receiver front end board to be installed at the Kapuskasing radar site

Another addition to the design came when it was noticed that some of the Mini-Circuits switches used as T/R switches needed the complement to the T/R signal. Creating this complement was accomplished by using a logic inverter chip mounted on a small printed circuit board that can be seen mounted on the board in the bottom right of Figure 2.6. For ease of changing out a bad chip, a chip socket was mounted on the board and the chip plugged into the socket. Using this inverter chip also became useful during field testing when it was realized that the TX On logic for the Mini-Circuit component was inversed from the current logic for the TX On signal. A high TX On signal, normally meaning the RF pulses can be passed to the transmitters, meant turning off the variable gain Mini-Circuits amplifier. As a solution, the TX On signal was routed through the inverter chip and then to the variable gain amplifier. This allowed the receiver board to interface with the current logic setup without having to redesign any of the electronics outside of the board.

2.3.3. Tests and Results

Upon completion of the board's construction, AC power was applied and the power supplies were tested for correct wiring and voltage levels. Next, a piece by piece analysis was conducted on the system components found in the block diagram in Figure 2.5. The results from the analysis of gains and losses through each system component of the receiver board can be seen in the block diagram in Figure 2.7. As can be noted from the figure, a few attenuators were added to the system for the proper operation of the board. Also, the bandwidth of the filters was slightly larger than the design called for, but these larger bandwidths do not effect the operation of the receiver board.

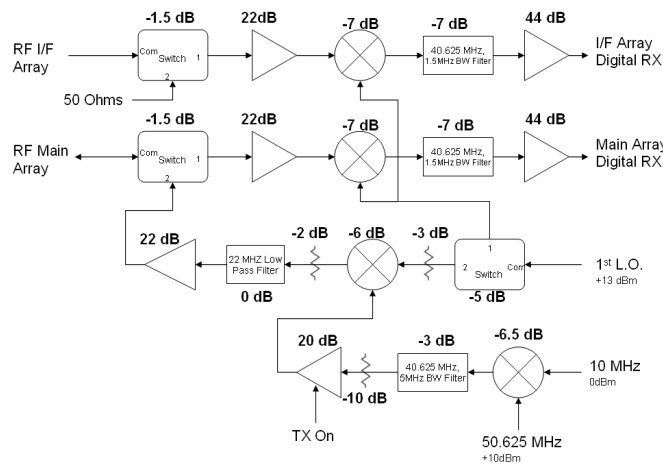


Fig. 2.7 Gains and losses on system components of the receiver front end board

The variable gain amplifier driven by the TX On signal in the bottom of the figure has a maximum gain of 20 dB when the TX On signal is high. When the TX On signal is low, this amplifier becomes a 10 dB attenuator. Another important part of the gains and losses through the receive side is that the main and interferometer array paths are identical. The identical gain allows for the strength of the signal between the two arrays to only be a

factor of the antenna gain. The two identical paths also allow for the phase delay of the two signals through the receiver front end to be close to identical for both signals.

Next an overall system analysis simulated the operation of the receiver board at a radar site by introducing the required first LO signal and a simulated constant frequency RF source into the receiver section of the board. The gain of the two paths on the receiver side showed a gain of about 54 dB from the RF input to the IF output. Using laboratory test equipment, the receiver is sensitive to -125 dBm for RF signals and is able to amplify them up to an IF signal level of -68 dBm. Often times, sky and thermal noise of RF environments have signal levels of -100 dBm and so an RF signal of -125 dBm will be below the noise. On the other end of RF signal levels, the receiver begins to saturate for RF signals higher than -50 dBm. At this RF signal level, the IF signal level is about +4 dBm which is close to saturating the digitizing computer card input. On the transmit side of this board, with the signal levels for the first LO, 10 MHz, and 50.625MHz as shown in Figure 2.7, the pulsed RF output from this board is about 15 dBm.

With these tests completed, the receiver front end board was temporarily installed at the Blackstone radar in July 2009 and ran for several weeks with some modifications to work with the Leicester electronics. These modifications involved the use of additional attenuators and adding another amplifier to the first LO signal. Also, a small design change was made during the test at Blackstone. The first LO signal path changed such that the mixers on the receive side are always fed with the signal and never switched. The first LO signal remained gated by the switch on the transmit side as seen in Figure 2.8. A quick glance through the data from these weeks showed that this

receiver board performed similar to the Leicester electronics. The ground scatter return power levels and distances and noise levels observed with this receiver board were comparable to returns and noise level observed using the Leicester electronics.

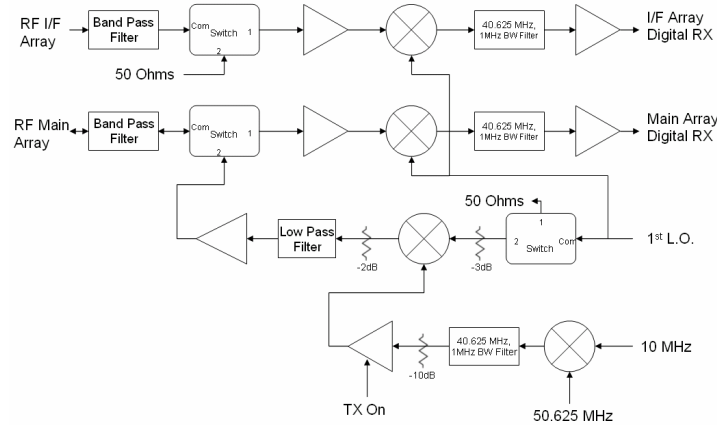


Fig. 2.8 Receiver board design with minor changes, addition of bandpass filters and changes to L.O. signal routing, as tested at Blackstone and installed at Kapuskasing

The board was then installed at the Kapuskasing radar site. One last addition to the board was made during the installation of the receiver board. Bandpass filters, made up of a high pass filter with a cut off frequency of 8 MHz and a low pass filter with a cut off frequency of 22 MHz, were installed on each of the RF ports on the receiver board. The high pass filter blocked out strong AM broadcast stations and the low pass filter blocked out strong FM broadcast stations. These filters help eliminate any potential higher order mixing products in the receiver.

This analysis of the receiver front end installed at Kapuskasing provides insight and performance specification for the design and fabrication of a standard SuperDARN receiver front end.

2.4. Transmitter Test Setup

The radar electronics at the Blackstone site were installed with the understanding that eventually the equipment would be replaced by our own equipment and the Leicester equipment returned. Part of the transition of replacing electronics is installing new transmitter units, pictured in Figure 2.9, in place of the Leicester transmitters. The new transmitters are a modified version of previously used transmitters and have been untested in the field. 18 of the new transmitters were delivered to the lab from SiL Inc., of Saskatoon, in order to be tested as a suitable replacement at Blackstone and for use at future radars.

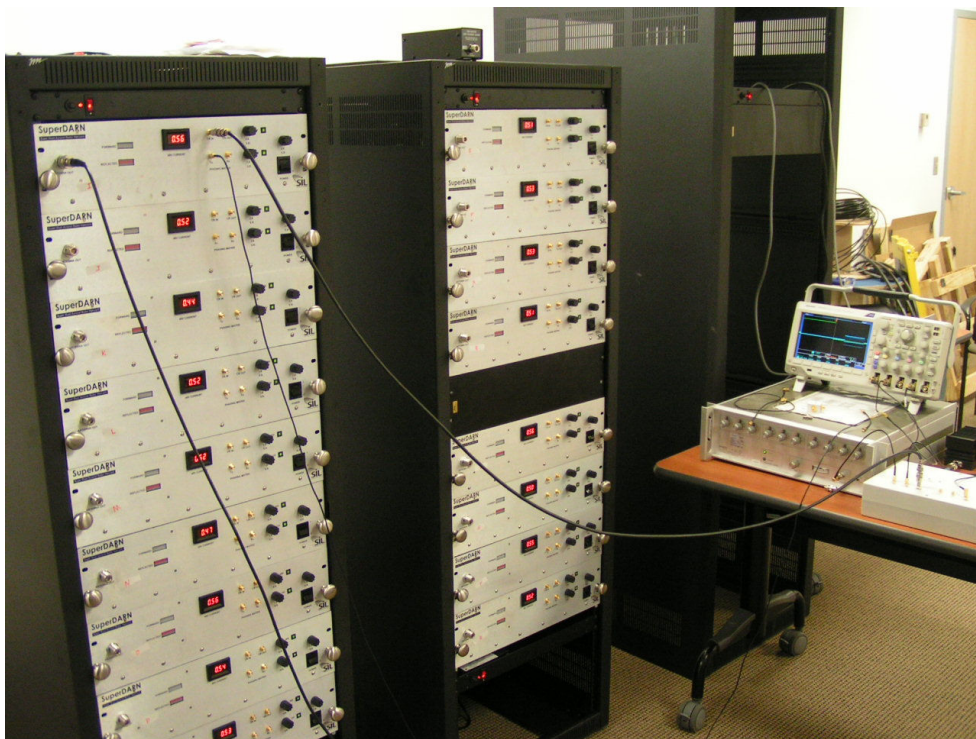


Fig. 2.9 Transmitters in the rack that will replace the Leicester transmitters at the Blackstone site

One test required the transmitter to prove its ability to make power under general radar operating conditions. These conditions required the transmitter to take pulsed RF signals along with T/R signals and create high-power pulsed RF signals. For initial testing purposes, the full setup for the radar electronics was not available and so a stand alone unit was designed, built, and tested.

2.4.1. Design

The general radar conditions used in the design of the transmitter test unit are listed in Table 2.1. As one common solution to timed pulses, Ellen Pettigrew, a doctoral student from the SuperDARN group at Dartmouth University, designed a circuit using integrated circuits timers. These timers allow for adjustable pulse widths as well as synchronizing chips through a trigger input.

Pulse Repetition Interval (PRI):	100 ms
T/R pulse width:	500 μ s
TX On pulse width:	300 μ s
TX On delay:	\sim 50 μ s

Table 2.1 General SuperDARN radar transmission and control signal characteristics

The resistance values and triggering connections as designed by Pettigrew can be seen in the schematic in Figure 2.10. The design allows for three signals to be varied with adjustable resistors in R1, R8, and R9. These adjustable resistances allow for the PRI, TX On pulse width, and T/R pulse width, respectively, to be changed for a more flexible test unit. The delay between the T/R pulse and the TX On pulse is fixed in this design by the value for R5.

From this schematic, I developed a unit that runs on batteries, takes a constant RF signal in and returns a pulsed RF signal. The pulsed RF signal is created by driving a coaxial switch contained in the test unit with the TX On pulse. This unit outputs a T/R signal so that the transmitter can be synchronized with the test unit. Outputs of the duty cycle, fixed delay, and TX On pulse are also provided as pictured in Figure 2.12. The user can adjust the variable resistors through openings in the unit and simultaneously monitor the signals.

2.4.2. Results

The design was built with no adjustments and the resulting waveforms were captured as shown in Figure 2.12. The top trace shows the duty cycle line dropping to 0 V and triggering the other timers. The next trace down shows the fixed delay pulse that upon a downward edge triggers another timer which is the TX On pulse and its trace is labeled TX On. The trace at the bottom is the T/R pulse that is triggered from the downward edge of the duty cycle pulse. As noted in the design, 3 of the pulses can be adjusted depending on the specification of the pulses generated. The duty cycle pulse can be adjusted such that it will have a downward triggering edge every 7 ms at the shortest and 150 ms at the longest. The TX On pulse can be adjusted to have a pulse width between 0 ms and approximately 11.5 ms. Since the timer generating the T/R pulse is the same circuit as the TX On except for the trigger input, the T/R pulse can also have a pulse with between 0ms and approximately 11.5 ms. The fixed delay pulse width was measured to be 172 μ s.

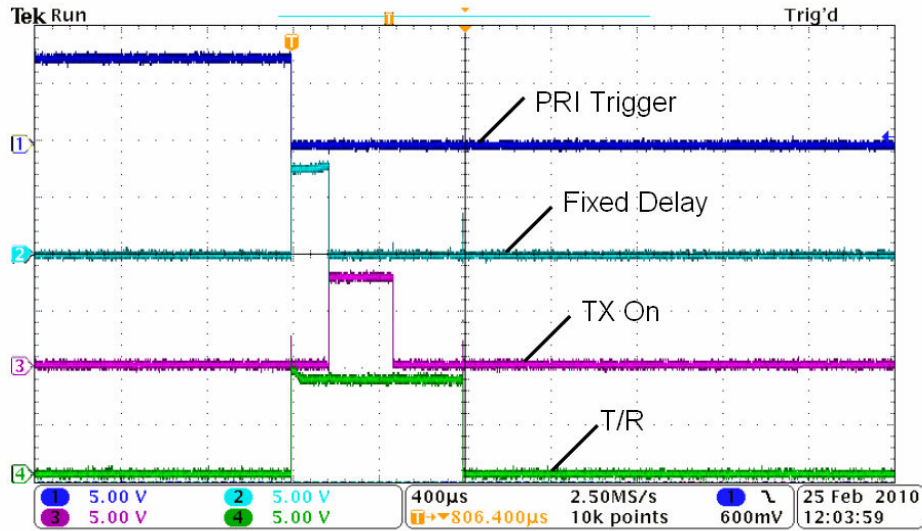


Fig. 2.12 Resulting waveforms for the transmitter test unit.

Each of these pulse width ranges fall within the specifications of the design listed in Table 2.1. This unit was then successfully used to send pulsed RF signals along with synchronized T/R pulses to a transmitter. The output of the transmitter was connected to a Wattmeter and then to a dummy load. The Wattmeter was able to read average power and peak power. With the low duty cycle of the pulse unit, the average power read on the meter was close to 0 Watts, while the peak power was about 600 Watts. The maximum peak power level of each transmitter varied about 50 Watts but this is acceptable for installation at the Blackstone radar. The output of a transmitter was also connected to an oscilloscope through attenuation and the transmitted waveforms were observed. The transmitted waveforms did not show any distortion from clipping as though any part of the transmitter was being overdriven. The output waveform resembles the input waveform by having some slight ramp-up and ringing on the RF pulse. These effects are due to the way the circuit creates the RF pulse with a coaxial switch.

This transmitter test unit that I built will be copied and distributed to current radar sites as part of standard test equipment to be used in testing the transmitters. The test unit will also be distributed to future radars being built as an expansion of SuperDARN.

2.5. Antenna Array Construction

I participated as project engineer in the construction of a previously untested layout of two radars at one site in Hays, Kansas. As project engineer, I dealt with several design and fabrication issues with the antenna array arose during the construction process and in the field. The radar construction at the Hays, Kansas site will serve as the model for the process in which planned SuperDARN radar builds in Oregon in 2010, in the Aleutian Islands in 2011, and in the Azores in 2012 will follow.

An analysis of antennas and their relation to this project and past antennas will be covered in the next chapter. In this section, the design and challenges of the hardware and construction of an array of TTFD antennas will be presented. Specifically, information presented here covers the experience of building the two TTFD-based radars at the Hays, Kansas, radar during the Summer and Fall of 2009. A summary of the construction process, details of which will follow, can be found in Figure 2.13.

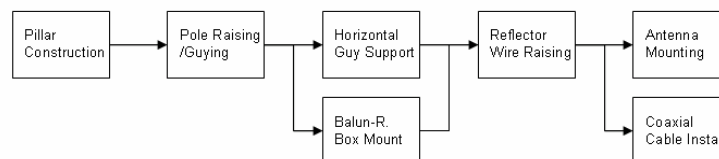


Fig. 2.13 Process of building a SuperDARN antenna array

The construction of the array started with surveying the piece of land designated for the SuperDARN site. Each array requires the land to not vary in elevation more than about 5 feet along an 800 foot straight path. Finding this length of relatively flat land was not very difficult in Hays, Kansas. The land grade requirement is set so that elevation of concrete pillars can be kept the same while not having the height of the concrete pillar too far above the ground which would begin to increase the cost of the construction and complicate antenna servicing. Before the concrete for the pillars has set, four threaded rods in a box configuration are set into the pillar and precisely lined up with each other so that each threaded rod will line up with the holes on the base of each pole as pictured in Figure 2.14. The process of digging holes for the pillars, pouring concrete, and setting the threaded rods took about a month in the Summer 2009. Once the concrete is poured, it is allowed to cure for another month before the next part of the construction, pole raising.



Fig. 2.14 A concrete pillar with threaded rods with an assembled pole ready to be raised and mounted on the pillar.

Next, each pole is assembled; each antenna support pole is made of up two smaller sections which are bolted together with a plate that serves to support the balun and resistor boxes as well as for attaching horizontal guy cables. Fitting the two sections of

the pole together was not always easily accomplished and a wax lubricant was applied along with a bit of brute force from a mallet. In preparation for the poles to be raised, four already prepared Kevlar guy cables were attached to the top of the pole. The Kevlar cable is used because of its strength and its non-metallic composition. Metallic cables, such as steel wire, would cause unwanted effects to the radiation pattern of the antenna (more will be covered in the next section about these guy cables). Once the poles were assembled, each pole was raised vertically and placed on each of the concrete pillars and secured at the base. The poles were secured at the top with Kevlar guy cables attached to the ground which also support the reflector antenna wires. These guy cables are pictured in Figure 2.15 with most of the poles raised at the Hays radar site.



Fig 2.15 Most of the antenna poles positioned with the guy wires temporarily tied into the ground anchors at the Hays site

2.5.1. Guy Wire Support

The four guy wires made of Kevlar fibers attached to the top of each pole were attached to the base of an adjacent pole or to a ground anchor through a turnbuckle. The guy cables attached to the ground are cut longer than required and left without a loop to connect the cable when the cables were prepared. This loop-less end will eventually attach to a ground anchor, but because of the variations in the ground level, the extra guy cable length was left on until the wire was ready to be attached to the ground. Leaving the extra length on the guy cables and cutting them as they were being attached allows for them to not be assigned to a specific guy anchor. The turnbuckle on the lower side of the four guy cables that connected to the top of the pole allowed for the position of the top of the pole to be adjusted and secured so that the pole did not vibrate too much in the wind. Positioning the poles and cutting the guy cables to length posed challenges at the Hays radar since the front and back guy wires needed to be cut and secured at the same time. The position of each pole is determined by a person operating a transit who must call out the adjustment that must be made. Calling out these commands was complicated by the lengths of the array as well as by high winds. The guying structure is integral to the design of the antenna array, as the guy cables support the antenna and reflector wires as well as for pole stability.

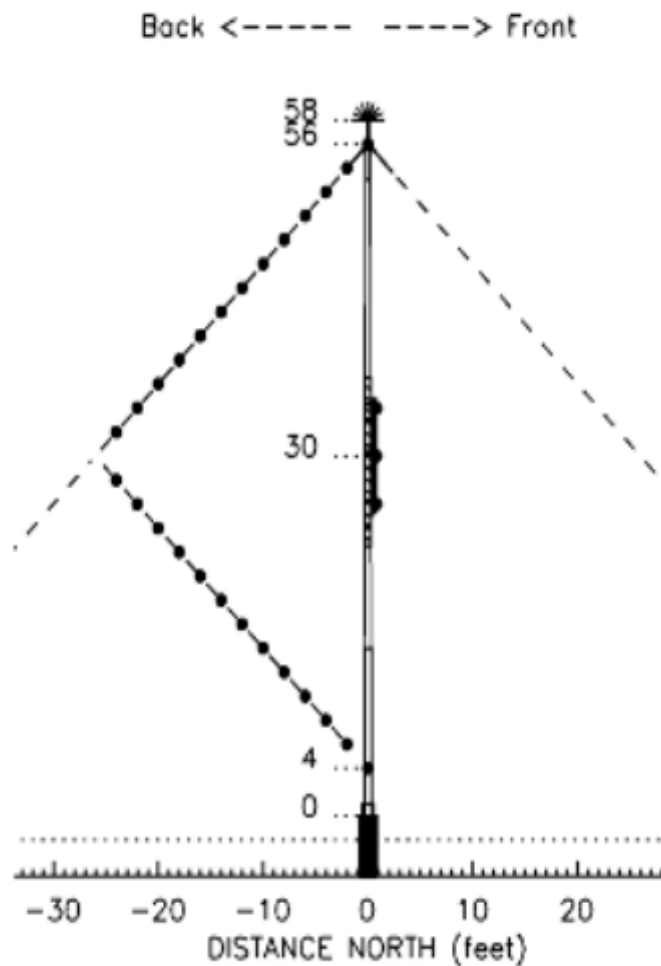


Fig. 2.16 A side view of the guying and wire construction of the TTFD antenna array

The guy cable on the back of each pole is actually made of two guy cables with a third guy cable attaching to the base of each pole. This arrangement of the cables allows for the corner reflector of the array to be constructed as can be seen as long dashed lines with dots in Figure 2.16. The three guy cables off the back of the pole, along with the guy cable off the front of the pole, are tensioned to the point that the guy cables do not sag under the weight of the reflector wires.

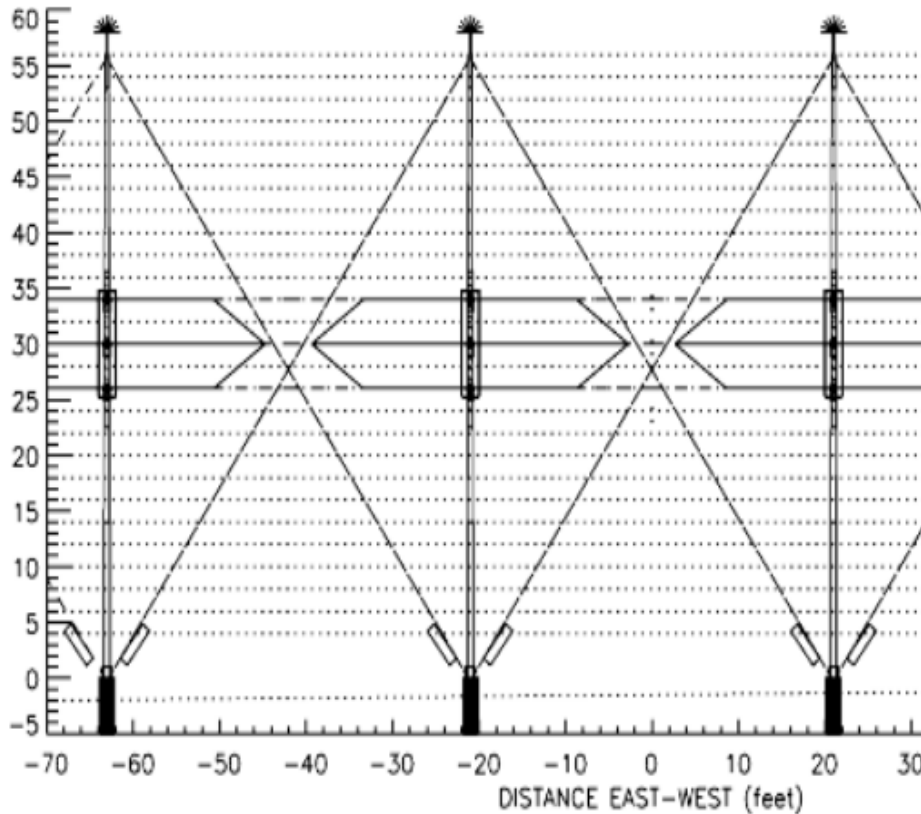


Fig. 2.17 A front view of the guying and antenna wire construction of a TTFD antenna array. The hexagonal shape of the TTFD design can be seen in the middle of the figure.

The last set of guy cables installed for the TTFD antenna array are three horizontal cables, seen in Figure 2.17 as the dashed lines in the gaps between each pole, which support the six-sided shape of the TTFD antenna. Each cable is pre-cut, measured, and marked on each end on the ground so that the markings will help align the cables with the poles and keep the cables consistent along the array. The measurements for cutting and marking an example horizontal cable are noted in Figure 2.18. With the cables marked and the poles mounted on the concrete pillars, the horizontal guy cables are mounted on the poles using a lift.

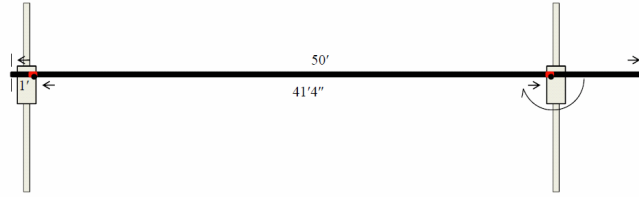


Fig. 2.18 Installation of the horizontal cables with markings shown

As seen in Figure 2.18 and pictured in Figure 2.14 each mounting plate has three widened sections at heights of 26’, 30’, and 34’ from the base of the pole. These rectangular sections are machined with holes that allow large bolts to pass through without threading. The horizontal guy cable is looped around bolts at one end of the cable and the bolts tightened in order to secure the cables to the poles. A completed attachment of the horizontal cable to the plate is pictured in Figure 2.19. The same action is repeated on the other end of the cable being sure to keep the marking on this side of the cable lined up with the edge of the plate.



Fig. 2.19 The installed horizontal guy wires as well as a resistor box.

Performing this part of the installation presented no surprises during the Hays radar build. First, the middle horizontal guy cable was attached in every gap between poles of the array. At each end of the array, an additional guy cable ran from the middle of the end pole to a ground anchor. Tensioning was applied to straighten out the middle

of the end pole as well as to secure the middles of the poles across the array. However, with the length of the array at about 750', a precision of better than a couple of inches in the middle of the pole could not be accomplished. The top and bottom horizontal guys were then mounted on the array. The process of installing the horizontal guy cables was done at the same time as baluns and resistor boxes were mounted to each antenna pole. These boxes were mounted at this time since the process of raising the poles could potentially damage baluns and resistor boxes. The biggest challenge of mounting the baluns and resistor boxes was using a lift to get up to the required height on sometimes uneven ground or in windy conditions. Despite these conditions, the poles were successfully secured and an adequate antenna supporting structure was formed by the Kevlar guy cables.

2.5.2. Reflector Wire Construction

In addition to the 6-sided shape of the TTFD antenna, a series of horizontal conductors are run behind the antennas along the full length of the array. These conductors are held in place by the Kevlar guy cables and spaced such that at the operating frequencies, the wires appear as a solid surface. The TTFD antenna array has been constructed at three different radar sites: Wallops Island, Blackstone and Hays. At each of these sites, the reflector wire portion of the antenna array is constructed slightly differently as the design at each radar has been analyzed and improved upon for the next radar built. The Hays radars are the last of the TTFD antenna arrays constructed and thus represent the best design of the reflector wire construction.

The conductors for the reflector wires are made from 13-gauge copper clad steel covered in a black polyethylene jacket and called PolyStealth. The copper clad steel

allows for the reflector wire to undergo high tension without stretching or breaking. Once the guy cables are set as described, hog rings are attached to the guy cables at each end of the array as well as every third guy cable along the array. This hog ring attachment used two sizes of hog rings as seen in Figure 2.20. The hog rings are placed along the guy cable at a regular spacing down the guy wire. This process is repeated until 12 of the hog ring attachments are along the top guy wire and 8 along the bottom guy cable making one for each reflector wire. The top hog ring is left open until a reflector wire is placed into the ring.

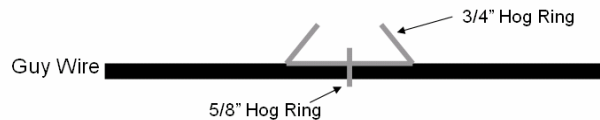


Fig. 2.20 Hog ring attachment to the guy cables using two sizes of hog rings

Next, the reflector wires are attached to an eye-nut that is secured to a slanted bar at one end of the array. This slanted bar matches the angle of the top guy cable and is pictured in Figure 2.21. As seen in the picture, another slanted bar is used to attach the bottom reflector wires. The reflector wire is secured to the eye-nut by putting the wire through the eye-nut and folding the wire back on itself. Then about five hog rings are crimped around about a foot of the wire that is folded back in order to form a secured loop through the eye-nut.

For simplicity, the top and bottom sections of the reflector wires are installed separately. Each of the 12 top reflector wires is pulled off of the spool the length of the array along the outside of the guy wires. This allows for the reflector wires to be pulled up along top of the guy cables and the reflector wires to sit on top of the guy cables.

However, with 12 wires pulled out along the outside of the guy anchors, the reflector wires can become easily tangled. Spotters on the ground are required in order to ensure that the reflector wires are kept in order. Physically, it was also a challenge to raise the slanted bars to their mounting positions on the end poles.



Fig. 2.21 The slanted bars at one end of the Hays radar with reflector wires attached

Starting from the top and working down through the 12 wires, each of the wires is placed in its corresponding open hog ring as noted in Figure 2.20 and then the hog ring is

crimped. This hog ring is large enough so that when it is fully crimped it will not crimp down onto the reflector wire. The crimped large hog ring allows the wire to move horizontally without pulling on the guy wire. The same process is repeated for the bottom 8 reflector wires except the wires are pulled off of the spool inside of the reflector near the base of the pole. The wire is pulled off in this way so that the reflector wire sits on top of the guy cable. Finally, one wire is pulled through the back eye-nuts on the top of each pole. Putting this top wire on allows for a reflector wire to be placed over top of the TTFD antenna and is critical for antenna performance. The bottom part of the corner reflector can use fewer wires than the top part since modeling has shown that additional wires on the bottom of the corner reflector do not significantly improve the antenna performance. Leaving out these additional wires saves on cost and allows the land around the TTFD antenna array to be more easily maintained.

This process for raising the reflector wires was the final method that was used during the Hays radar build. The original idea for raising a reflector wire involved attaching a wire at one end to the slanted bar and then pulling the other end of the wire tight and attaching this end of the wire. This method was successfully demonstrated on the interferometer array which is shorter in length than the main array. Attaching both ends did not work on the main array because a person in a lift pulling on the second end of the wire could not keep the reflector wire from getting caught on the large, open hog rings. The method described previously of attaching one end and working along the array with the wires was improvised among a collection of people including myself at the Hays radar.



Fig. 2.22 Tangled or loose reflector wires along one section of the TTFD array at the Hays radar in Feb. 2010

In the months since the construction of the Hays radar, several reflector wires on one part of the array have come loose and tangled as pictured in Figure 2.22. In addition, another reflector wire along the bottom of a different part of the array snapped. It is suspected that the crew used too-large hog rings for clamping on the guy wires on this one array. The problem will be investigated in the Summer of 2010.

2.5.3. Antenna Construction

Antenna wires are prepared on the ground before being mounted on the horizontal guy wires. Each antenna can be divided in half since the shape of the antenna is symmetric around the pole. Each half is made up of three lengths of wire as seen in Figure 2.23. The top and bottom lengths of wire are the same and are the sum of the 12 feet, almost 7 feet diagonal, as well as the 3 inches coming back to the middle length of wire. For overlap, the top and bottom lengths are cut to 19 feet, 3 inches and the middle length is cut to 17 feet, 9 inches. The wire used for the antenna wires is a 12-gauge, 259

strand annealed bare copper with a black polyethylene jacket called Flex-Weave. The large number of strands allows the wire to be flexible enough to create the sharp bends formed in the TTFD shape.

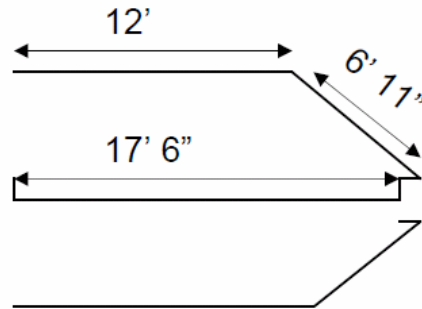


Fig. 2.23 Dimensions of half of a TTFD antenna

With the three wires cut, an inch of insulation is cut away on each end and an eye terminal attached to one of the two ends. This eye terminal allows each wire to be connected to the threaded terminals of the resistor boxes and baluns. The three other ends are joined electrically through a crimped metal ring. This connection is then sealed in heat shrink to prevent water from entering the joint and corroding the metal.

The completed antenna halves are mounted once the horizontal guy wires have been completely installed. First the eye terminals of each half are connected to the respective resistor box or balun. Then with hog rings, the middle wire is secured every 3 feet along the middle guy cable without letting the antenna wire sag as pictured in Figure 2.24. A hog ring or two secures the 3 inch overlapping sections of the top and bottom antenna wires to the middle guy cable. Without bending the horizontal guy cables, the top wire is pulled tight along the top horizontal guy cable and the corner of the top antenna wire is secured with a hog ring. The top antenna wire is then further secured to the top horizontal guy every 3 feet with a hog ring. The same procedure for the top wire

is repeated for the bottom wire. This installation process is then repeated for each half of the antenna along the array.



Fig. 2.24 The middle antenna wire being attached to the balun on the right and secured to the horizontal guy on the left

Telling the three wires from each other proved to be a small challenge during the installation as well as aligning the wire length on the correct corresponding horizontal guy cable. Another difficulty encountered while mounting the antenna wires to the horizontal guy cables was dropping the small washers and nuts from the baluns and resistor boxes. Extra parts did not come with the baluns and resistor boxes and needed to be replaced in the field. These nuts and washers were available at local hardware stores and all of the antenna wires were ultimately attached properly with the correct hardware.

As noted in Figure 2.13 at the same time as the antenna wires were being mounted, the coaxial cables for carrying RF signals to the antennas were installed at the Hays radar. Starting from the antenna, a 30 foot length of LMR-600 type cable was connected to the balun. Every 6 feet down the pole the cable was attached to the pole

using a coaxial cable hanger specifically designed to fit around LMR-600 type cable. The hanger was held to the pole by using a hose clamp that fits around the pole and slid through openings in the hanger. This 30 foot cable connected to the buried coaxial cable which connects to the transmitters in the building. Each buried cable was cut to the longest length required to reach from the building to the farthest antenna pole for each array. At the Hays radar, the two-radar layout required each of the main array buried coaxial cables to be approximately 800 feet long. The long length requirement for these cables led to the use of low loss LMR-600 type cable which has a loss of about 0.4 dB per 100 feet at the radar operating frequencies. Once all of the cables for an array were unspooled and before the cables were buried, each was measured for its electrical length. This was accomplished by using a network analyzer on one end and leaving the other end as an open circuit. In this configuration the network analyzer was able to measure the phase of the reflected signal and the electrical length could be computed using two phases from two wavelengths and the propagation factor of the coaxial cable. Each cable was then re-cut and a connector placed on the building end, as pictured in Figure 2.25, so that all of the cables were the same electrical length. Excess cable length was coiled up in 15' x 15' x 4' pits dug for this purpose near the equipment shelter.



Fig. 2.25 Coaxial cable entering the building from one radar and connectors being attached

The construction of the two Hays radars was completed in November 2009 and data from one radar was recorded shortly thereafter. I spent 3 weeks in total, a week in late September and another 2 weeks spanning October and November, overseeing the project. The second radar was operational in November, but due to software issues, both radars could not stably run at the same time. These software issues were corrected in February 2010. To date, the pair of radars have provided the SuperDARN research group with good, sensible data as seen in Figure 2.26 to extend studies in ionospheric physics and space weather.

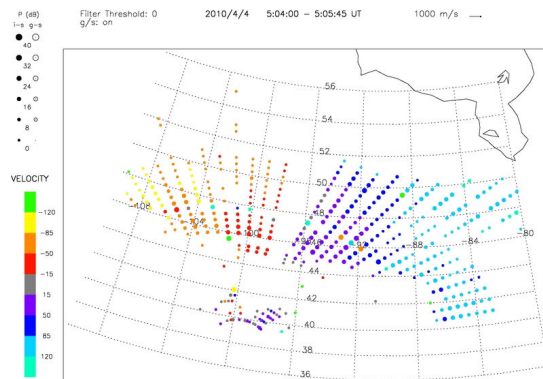


Fig. 2.26 Sample radar data from the two Hays, Kansas radars

3. Modeling the TTFD Antenna Design

In this section, modeling for the TTFD antenna design is presented as well as variations on the orientation of an array of TTFD antennas. The TTFD antenna has become the antenna of choice for the SuperDARN radars built since 2004. Before this time, SuperDARN radars used a log-periodic antenna. The TTFD antenna costs less to fabricate and construct and has been implemented at several SuperDARN sites but has yet to be fully modeled. The work presented here shows modeling of a TTFD antenna and for the first time the results from a full antenna array model. These results are compared to a full array of log-periodic antennas.

3.1. Introduction

The numerical simulation of electromagnetic fields radiated from antennas began in the mid 1960s with the development of integral equations by Roger Harrington, Jack Richmond, and Ken Mei. These equations became the basis for several computer algorithms developed by U.S. military research labs over the next decade. The first of these algorithms used pulse basis functions, point matching, and a method of moments solution of Pocklington's Integral Equation which gives the solution of a radiated electric

field given a current along a wire and a Green's function. This equation is developed under the assumption that the wire is thin compared to the wavelength of the fluctuating current and that the wire is straight. The code was further developed in 1967 and called BRACT. This algorithm used a three-term basis function developed by Mei in point matching solutions of Hallen's Integral Equation which provides for a sinusoidal current expansion. An explanation of the basis function will be presented in the next section. A year later, BRACT became ANTBRACT by including the ability to put voltage sources on wires and use of the Reflection Coefficient Approximation to approximate a ground plane.

Interest in modeling algorithms of antennas was pursued in the early 1970s by several military research laboratories. In 1971, the developers of ANTBRACT, MBAssociates, won a proposal competition from these laboratories and developed the Antenna Modeling Program (AMP) in 1972. AMP was much like ANTBRACT but AMP had a friendlier user interface and a large user manual. However, the simulations required long computation times and AMP was modified five years later to use approximations when the observation and source points exceeded a specified value. The new program, called AMP2, used thin-wire approximations for the electric field integral equation (EFIE) for wires and the magnetic field integral equation (MFIE) for voluminous structures.

Within two years, the popularity of AMP and AMP2 led researchers at the Air Force Weapons Lab to further develop the code by improving the current basis function and using an extended thin wire kernel. This development led to the first of many versions of the Numerical Electromagnetics Code (NEC). NEC also included a new

model for a biconical voltage source which will be described in a later section on sources. A few years later in 1981, NEC2 was developed in response to a need to model antennas near realistic grounds. This version of NEC solved this need by using Sommerfeld Integrals for the interactions of the field with grounds and an interpolation technique to provide accurate but faster solution of the Sommerfeld Integrals for wire antennas. These integrals and the interpolation technique will be described more in the next section.

More versions of NEC have been developed to accommodate antennas that include wires buried in or penetrating a ground plane. The latest version of NEC, NEC4, was developed in 1990 and allows for the modeling of wires with insulation, non-constant radius in the wires, and wires buried in the ground. However, these features of NEC4 are not necessary for the modeling of the TTFD antenna array since no antenna wires are under ground, no tapered wire thicknesses are used, and the insulation on the wire is thin, in the millimeters range, in comparison to the wavelength, around 100 feet. The NEC2 version of the code served our needs in modeling the TTFD and log-periodic antenna arrays.

NEC2 was developed in 1981 from a series of earlier computer algorithms that simulated the radiated fields of wires and surfaces that were excited by currents. The version developed at the Lawrence Livermore Laboratory by G. J. Burke and A. J. Poggio [21] included algorithms that used a quicker computational method by incorporating the EFIE in combination with the MFIE.

3.2. The Numerical Electromagnetics Code (NEC) 2

The EFIE is used when the structures follow the thin wire approximation [22], namely for thin wires. The equation can be used to represent thin surfaces if the surface is converted into a grid of thin wires in the program. The EFIE is defined as:

$$-\hat{s} \cdot \vec{E}(\vec{r}) = \frac{-j\eta}{4\pi k} \int_L I(s') \left(k^2 \hat{s} \cdot \hat{s}' - \frac{\partial^2}{\partial s \partial s'} \right) g(\vec{r}, \vec{r}') ds',$$

and,

$$I(s)\hat{s} = 2\pi a \vec{J}_s(\vec{r}), \quad g(\vec{r}, \vec{r}') = \frac{e^{-jk|\vec{r}-\vec{r}'|}}{|\vec{r}-\vec{r}'|}, \quad k = \omega\sqrt{\mu_o\epsilon_o}, \quad \eta = \sqrt{\frac{\mu_o}{\epsilon_o}}$$

where \hat{s} is the unit vector tangent to the wire axis at \vec{r} , $\vec{E}(\vec{r})$ is the radiated electric field, s is the distance parameter along the wire axis at \vec{r} , a is the radius of the wire, $\vec{J}_s(\vec{r})$ is the surface current on the wire, \vec{r} is the radial vector from the wire, \vec{r}' is the vector to the observation point, μ_o is the permeability of free space, and ϵ_o is the permittivity of free space. The equation is best suited for structures with dimensions up to several wavelengths in order to properly apply expansion functions, although the equation does not have a theoretical size limit. The numerical solution to this equation requires a matrix equation which increases with order as the size of the modeled structure increases. Large structures in comparison to wavelength will take more computational time because of these growing matrices.

The thin wire approximation is used when the wire's radius is much less than the wire length and much less than the wavelength [22]. The thin wire approximation has

been shown to introduce less than 1% error if $\frac{\Delta}{a} > 8$, where Δ is the length of the wire and a is the radius of the wire. Also, for the numerical solution to the EFIE, to obtain an adequate representation of current distribution ka must be less than 0.08, where k is the wave number. For the TTFD antenna array with the wire lengths in the tens of feet, the wire radius less than an inch and the wavelengths are between fifty and a hundred feet, the conditions for using this approximation are fulfilled. The assumptions used in the thin wire approximation are:

1. Transverse currents can be neglected relative to axial currents on the wire
2. The circumferential variation in the axial current can be neglected
3. The current can be represented by a filament on the wire axis
4. The boundary condition on the electric field needs to be enforced in the axial direction only

An alternate solution, based on an extended thin wire approximation, is used in NEC2 for wires with too large a radius in which the third assumption on the approximation is neglected.

3.2.1. Method of Moments

The equations are numerically solved by using a method of moments technique similar to the technique described by R. F. Harrington [23]. This technique divides up wires into smaller straight segments and creates a current function along each segment. In each segment, the spatial center value for current is used to create a point sample of the integral equation. However, this method depends on creating an accurate function along the wires to represent the current. For modeling fields radiated by a wire, NEC2 uses a three term function as a basis function that is made up of a constant, a sine, and a cosine:

$$I_j(s) = A_j + B_j \sin(k(s - s_j)) + C_j \cos(k(s - s_j)), \quad |s - s_j| < \frac{\Delta_j}{2}$$

where s_j is the value of s at the center of segment j and Δ_j is the length of segment j . This basis function is used to describe the current along the segments on the wire as seen in Figure 3.1. An example of the total current is shown in Figure 3.2 for a half-wave dipole. As expected, the current is maximum at the center of the wire and goes to zero at the ends of the wire and follows a roughly sinusoidal pattern along the wire. The three term function was developed by Y. S. Yeh and K. K. Mei [24] and allows for the current to fulfill continuity conditions of current and charge at the segment ends. Fulfilling these conditions means that there are no discontinuities between segments, even at multiple wire junctions, which allows for an accurate representation of the current along the wire.

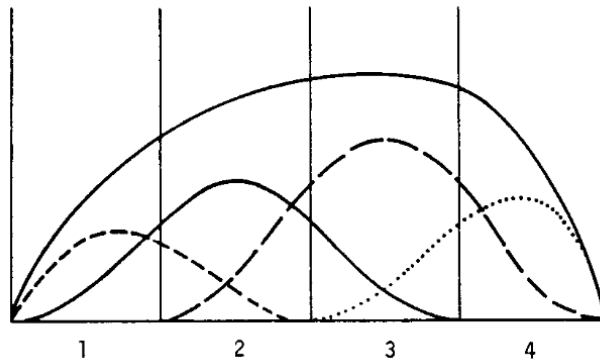


Fig. 3.1 The current expansion functions of a wire of four segments. The lower sinusoidal lines are summed to create the top sinusoidal line. [21]

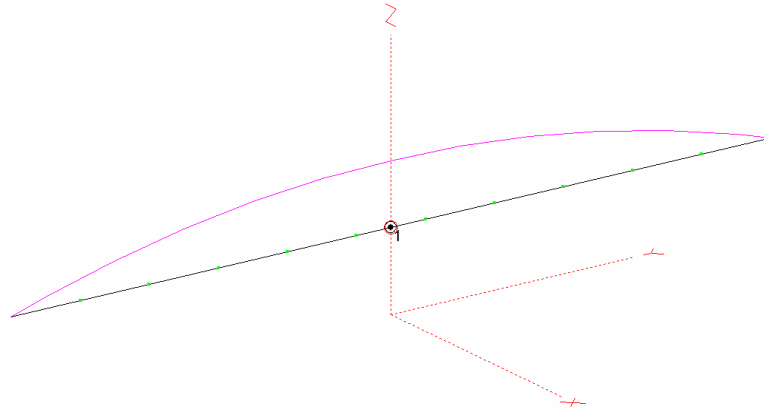


Fig. 3.2 The summed current along a half wave dipole antenna with a center fed current source.

3.2.2. Approximations

Three approximations are used in NEC2, the thin wire approximation, the extended thin wire approximation, and a current element approximation for large interaction distances. The thin wire approximation, its requirements, and its assumptions were discussed earlier. In the case that the model does not exactly fit the requirements for the thin wire approximation, NEC2 uses the extended thin wire approximation developed by Poggio and Adams [22]. This approximation uses a solution in terms of the radius of the wire squared and is used when the wire is too thick for an accurate solution using the thin wire approximation. The third approximation mentioned is used when segments are separated by a large distance. This approximation treats segments that are far away from the observation segment as infinitesimal current elements at the center of the segment saving computation time without sacrificing accuracy. NEC2 leaves the classification of a large distance up to the user, but is set to one wavelength by default.

From the approximations, the setup of the EFIE and the MFIE, and a known structure, NEC2 proceeds with the computation by setting up a matrix equation called an interaction matrix that is made up of submatrices. Using this form allows NEC2 to

separate the solution into parts that may be used repetitively for the same structure. These parts are then saved to a file and reused during a later run of the code when the structure is the same, but a different excitation is simulated. This process in NEC2 is called the Numerical Green's Function (NGF) option since it essentially replaces the free space Green's function with the Green's function on file for the particular structure. NEC2 is able to create a new NGF when a new structure comes in contact with the old structure by satisfying boundary conditions at the junction of the two structures. The use of the matrices also allows for the incorporation of structural symmetries which can reduce the computation time of a simulation.

3.2.3. Effect of Ground Plane

As mentioned before in the history of NEC2, one of the biggest modifications from the original NEC was a need to model antennas near a realistic ground. Introducing a ground plane changes the integral equations in three ways:

1. Modifies the current basis functions through near-field interactions
2. Modifies the fields illuminating wires and surfaces
3. Modifies the reradiated fields from these wires and surfaces

These three modifications ultimately affect the Green's functions in the integral equations. A solution to the integral equations in the presence of a ground plane comes from Arnold Sommerfeld [25], but the solution is computationally intensive. For quicker solutions, NEC2 uses different forms of image theory to solve for field interactions with a lossy and a perfectly conducting ground.

The most accurate method that NEC2 uses for the effect of a lossy ground is the Sommerfeld/Norton option which includes Sommerfeld's integrals for ground fields for a

small interaction distance and Norton's asymptotic approximations [26] for large interaction distances. The judgment for whether a distance is small or large in this case is whether the distance is shorter or longer than one wavelength. This method's code originated from another program called WFLLL2A. The time to compute the solution to the Sommerfeld integrals is reduced by creating a grid of values from the Sommerfeld equation and interpolating to fill the interaction matrix. Poggio and Burke note that the time to create the interaction matrix takes about four times longer than a similar solution for free space.

NEC2 allows the user to choose a faster solution to interactions with a ground plane by using image theory. For perfect conducting grounds, the solution using image theory is simple since the image is exactly the same as the source. For lossy grounds, NEC2 uses image theory along with Fresnel plane-wave reflection coefficients. Poggio and Burke note the solution is computed twice as fast using this method. However, the accuracy of reflection coefficients degrades for interaction distances that are closer than 0.1 to 0.2 wavelengths from the ground, but can provide practical results otherwise. The interaction distances with the TTFD antenna array fall outside of the qualification of too short since the shortest distance to the ground is at least 28 feet for the excited antenna (Wavelengths used for the radar are in the range of 75 to 100 feet). Reflector wires do not have much current running along them and are ignored for this classification even though most reflector wires are more than 10 to 15 feet above the ground. So Fresnel reflection coefficients can provide fairly accurate results for the TTFD antenna array. The coefficient formulas for various polarizations are included in NEC2 so the reflection coefficient for any field polarization can be computed. NEC2 also includes an

approximation to the coefficient formulas that may be used for radial wire ground screens.

3.2.4. Modeling Physical Antenna Components

As a final section, Poggio and Burke discuss how NEC2 models physical elements of an antenna other than wires such as sources, transmission lines, and loads. Sources are modeled one of two ways, the first of which allows for a constant voltage to be applied over the length of a segment on a wire. This creates a constant field over this segment which works well if the segments close to the source segment are all the same length. The admittance at the source can then be computed as the average of the current at the segment ends. If the current over the source segment length is not constant, NEC2 uses the second type of source, a biconical transmission line source. This source model allows for more variation of segment lengths near the source segment. However, segments adjacent to the source segment must have equal lengths and radii. Because the length of the wires in the TTFD antenna are on the order of the wavelengths used for this antenna, it is believed that the current over the source segment is relatively constant and uses the constant voltage source instead of the biconical transmission line source.

The modeling of transmission lines is important since many antennas are fed by a piece of transmission line. In NEC2, there are two ways in which transmission lines are modeled: explicitly by a thin wire model and implicitly as a two-port network with defined short-circuit admittance formulas. The implicit form does not include the interaction of the transmission line and the antenna. For balanced antennas and transmission lines in an electric symmetry plane, this is not a problem since the fields cancel out; however, for unbalanced antennas the implicit form does not work as well.

The explicit form uses similar computations that are used for antenna wires and thus takes longer to compute than the implicit form. No transmission lines were included in the TTFD antenna modeling since the TTFD antenna is a balanced antenna and the transmission lines do not affect the antenna's performance. In addition to transmission lines, NEC2 handles other multiple port networks by dividing the network into multiple two port networks.

Lumped or distributed loads on the antenna are easily handled in NEC2 by modifying the EFIE's boundary conditions to include imperfect conductors. Impedance in the EFIE can be treated as a constant field voltage source as previously discussed. The constant field source is used since it can be assumed that the current is roughly constant over the length of the resistive segment. Two loads are modeled in the TTFD antenna modeling since the antenna design calls for two resistive loads.

Antenna coupling is determined in NEC2 by using the Linville method [27]. This method determines the two port admittance by exciting one source with the other source short circuited. This procedure provides a measure of the amount of coupling between antennas in the case of multiple sources for multiple antennas.

3.2.5. Radiated Field Calculation

To calculate the radiated fields from an antenna, NEC2 uses far field approximations to simplify the EFIE. Even though it is generally accepted that a transmitting pattern is the same as a receiving pattern, NEC2 can use methods to separately model the two patterns. In order to determine the transmitting pattern, a voltage can be applied to the source to excite the wires. To determine the receiving pattern, a plane wave can be launched toward the antenna and the induced currents at the

source point can be computed. Poggio and Burke note that the patterns may differ because of different expansion and weighting function between the two methods. However, the patterns will be nearly the same unless too short or long, or non-uniform length segment sizes have been used to model the antenna. The effect in the far field of the ground plane goes away since the Sommerfeld equation reduces to the simplified EFIE mentioned before. NEC2 does allow for the calculation of ground waves through Norton's asymptotic approximations.

3.3. EZNEC

EZNEC, developed by Roy W. Lewallen in 2000, is the modeling program used in this thesis. The program uses the Numerical Electromagnetic Code version 2 (NEC2) as described before with a graphical user interface, pictured in Figure 3.3, which allows the user to input specific parameters. These parameters include wire endpoints, loads, sources, frequency, ground type and plot type. Here, wire endpoints are the way in which the geometry of the antenna is created by using straight pieces of wires. For curved antenna pieces, the user needs to input several smaller straight pieces to form the curved shape. Some error is introduced in this process, but the error can be small if the wire setup is done correctly.

EZNEC MODELING

- Prototype TTFD design
- 4-antenna Wallops TTFD model
- 4-antenna Blackstone TTFD model (effect of splice)
- 4-antenna Hays Kansas TTFD model (balun impedance mismatch)
- 8-antenna Falkland Island ground variations models, Log-periodics and TTFDs
- 16-antenna main array, 4-antenna interferometer array, Log-periodics and TTFDs

Table 3.1 Antenna models created and analyzed with EZNEC

In the TTFD design, no curved pieces of wire are used. Other conducting wires and surfaces that are not part of the antenna are inputted into the wire list since this list will be used while calculating the currents, impedances and radiated fields. Surfaces can be simulated by creating a wire grid as long as the wire spacing is small compared to the wavelength. The EZNEC program does not allow the entry of the “large” distance mentioned earlier for the NEC2 approximation for segments separated by “large” distances.

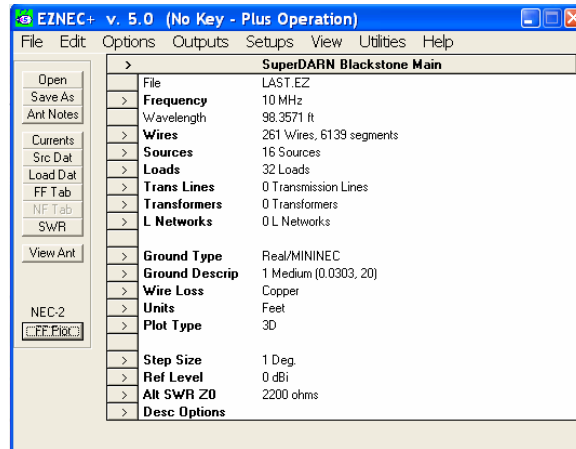


Fig. 3.3 The user interface for the EZNEC program

From the solutions of the NEC2 algorithm, the EZNEC program can create a far field antenna pattern in three dimensional space as well as tabular outputs of the far field and near field signal strengths. From plots of the far field pattern, basic characteristics like gain, beamwidth, side lobe level, and the front to back ratio can be determined. EZNEC can also allow a user to determine the standing wave ratio (SWR) at a source segment over a frequency range as well as allow the user to change the standardizing impedance used to calculate the SWR. With a capability of handling 20,000 segments, EZNEC Pro/2 v. 5.0 was used for the simulations presented in this paper.

3.4. Previous Simulation of the TTFD Antenna

Before a full SuperDARN radar array consisting of twenty antennas was built using the TTFD antenna design, a field test was performed at the University of Saskatchewan to ensure the modeled antenna matched actual radiation measurements [20]. This test was done to verify that the TTFD antenna yielded performance characteristics similar to those of the log-periodic antennas. The reflector was

constructed as a flat panel reflector as sketched in Figure 3.4. The wires that make up the reflector are close enough together that at the operating frequencies, 8-18 MHz, the wires look like a solid object.

EZNEC

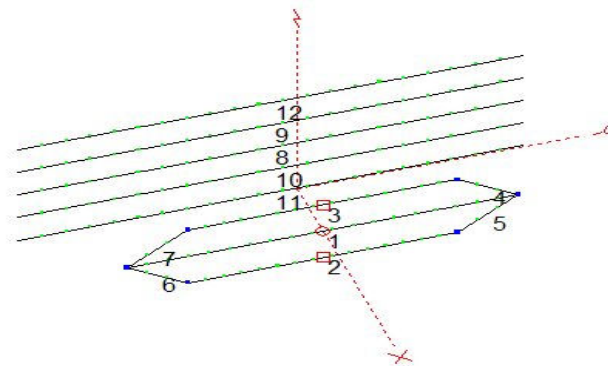


Fig. 3.4 TTFD antenna with reflector as modeled and tested at Saskatoon [20]

The simulated design placed the five horizontal wires 4.5 meters behind the TTFD antenna. As with the description of the TTFD before, the source was simulated in the center of the middle horizontal wire of the TTFD and is marked as a red circle. Two resistive loads are placed in the center of the top and bottom horizontal wires and are marked as red squares. The results of simulations using EZNEC showed that the TTFD design produced good radiation patterns and characteristics. The simulated pattern for the TTFD antenna design with the flat reflector can be seen in Figures 3.5 and 3.6. These figures present vertical and horizontal slices of the radiation pattern along with data about certain characteristics of the pattern. In particular, the value of 12.9 dB in Figure 3.6 for the front-to-sidelobe ratio shows the effectiveness of the five wire reflector.

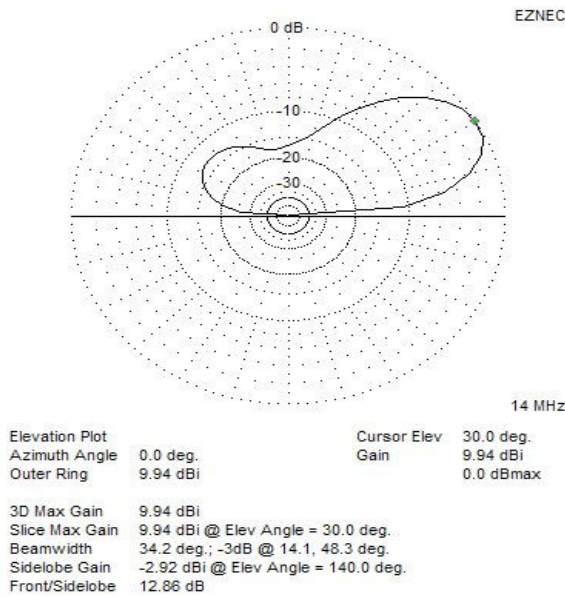


Fig. 3.5 Vertical Slice of TTFD Pattern[20]

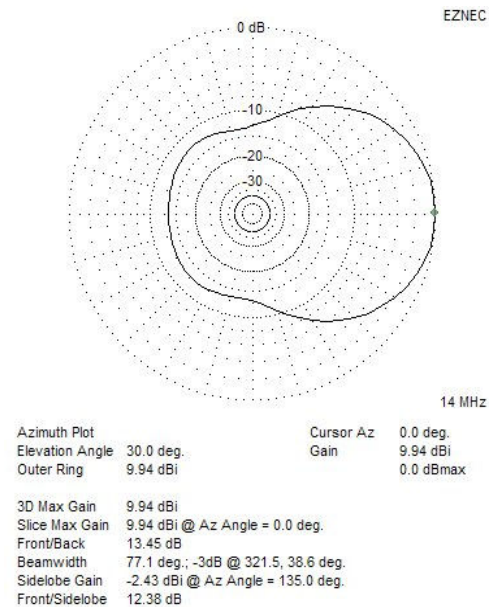


Fig. 3.6 Horizontal Slice of TTFD Pattern at an Elevation Angle of 30°[20]

With these results, the TTFD prototype antenna was installed in a full 16-antenna array layout at the Wallops Island radar site and eventually at other SuperDARN radar sites.

3.5. Twin Terminated Folded Dipole – SuperDARN

Two SuperDARN sites, Wallops Island and then Blackstone, Virginia, used the TTFD antenna design for the main and interferometer array. These arrays were built using 50' and 56' tall traffic poles, respectively, mounted on top of concrete bases. A corner reflector was developed to replace the 5 wire flat reflector design that was used in the previous section. The corner reflector was built in a similar fashion using horizontal wires spaced within a few feet of each other and running along the length of the array. A sample 4 antenna array is shown in Figure 3.7 with the horizontal reflector wires behind the antennas.

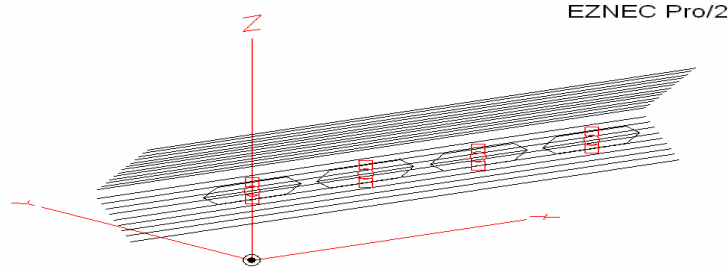


Fig. 3.7 An array of 4 TTFD antennas similar to arrays at Blackstone

As mentioned, the arrays at Wallops Island and Blackstone are not exactly the same. The Wallops Island array uses resistive loads of 100 Ohms, while the Blackstone arrays uses resistive loads of 75 Ohms. The change at Blackstone was made because of the excessive loss associated with the 100 Ohm loads. Also, the Blackstone radar incorporated more reflector wires than the Wallops antenna array. The corners at the far ends of each antenna also presented a challenge in implementation. At this junction, three wires come together and need to be joined.

At Wallops Island, a through-bolt was used to connect the three wires at the corner. At Blackstone the connection is made with a butt splice that is positioned on the center horizontal wire near the corner. This creates two wires running next to each other for a couple of inches until the wires reach the corner. At that point, one wire goes up to form the top of the antenna and the other goes down to form the bottom of the antenna.

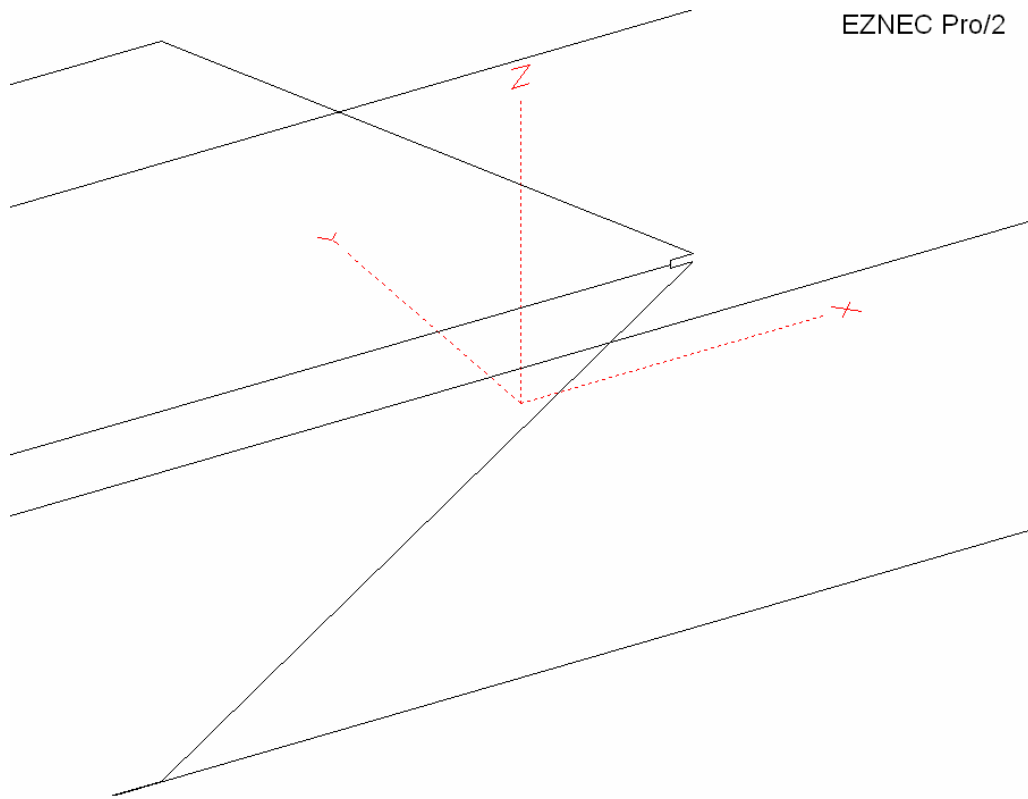


Fig. 3.8 An EZNEC model of the butt splice at Blackstone

A question arose about what effect this butt splice might have on the antenna's performance. The easiest way to find an answer to this question is to model the butt splice in EZNEC. A model of the butt splice in EZNEC is shown in Figure 3.8. From EZNEC, changes in the pattern characteristics can be noted, but cannot be verified without a complex and expensive measurement of the pattern as previously performed at Saskatoon. EZNEC also provides a standing wave ratio (SWR) plot across a frequency range for each source that is modeled. Differences in these plots can be compared and changes in performance can be inferred from the SWR values. An SWR plot also allows for a much simpler verification since an SWR meter can be attached to the coax break at the base of the antenna pole. To save on computational time, a 4-antenna model was used for initial tests and modifications. Later an 8-antenna model was developed for

variations on the layout of an array of TTFD antennas and lastly a full 16-antenna model was developed in the last section of this chapter.

3.5.1. Modeling the Effect of an Antenna Splice

As discussed before, there were some practical difficulties in implementing the TTFD design. To see the effect of the butt splice on the antenna's performance, two models were developed and used. One is an ideal antenna model that uses three wires joining at the corners of the antenna design. The other is an implemented antenna model that features the butt splice model as seen in Figure 3.8. It should be noted that the modeling of the butt splice creates three inch-long wires. This length of wire means that only one segment can be created on the wire which may lead to inaccuracies from improper current expansion. The length to radius ratio of these wires is around 10 to 15 and for the solution to have less than 1% error due to the thin wire approximation, this ratio must be greater than 8.

Based on construction diagrams, a model was constructed in EZNEC to resemble the constructed antenna. The wire end points were picked based on the figures as well as notes about the actual construction of the antennas. A sample of the wire end point coordinates and other wire parameters can be seen in Appendix A. The data for Appendix A is from a model developed for testing the ideal antenna structure as will be discussed shortly. The TTFD antenna is formed by wires 22 through 28 while the corner reflector, composed of 21 wires, is formed by wires 1 through 21. The number of segments was chosen in order to keep the segment length within the NEC2 guidelines for suitable segment lengths. However, due to the size and shape of the TTFD antenna, the segment length is not the same for all wires but is kept at about 2.5 to 3 feet throughout

all segment sizes. Also, the reflector wire lengths were chosen to follow the construction at Blackstone and Wallops. The number of segments per reflector wire was chosen to be close to the segment length of the antenna wires.

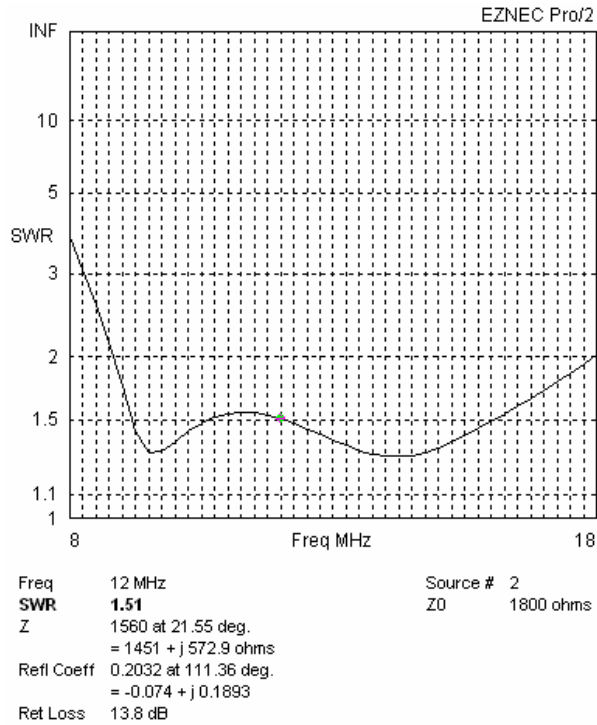


Fig. 3.9 Preliminary SWR plot of TTFD antenna model without splice, the ideal model

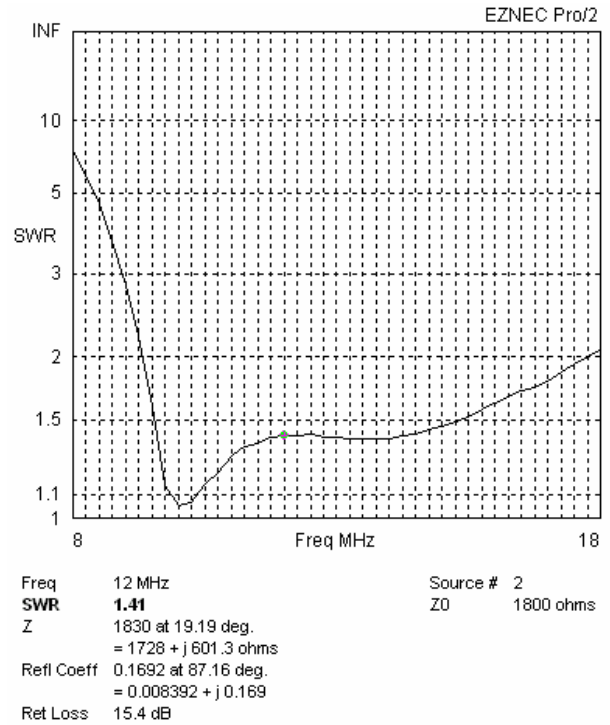


Fig. 3.10 Preliminary SWR plot of TTFD antenna model with splice, the implemented model at Blackstone

Modeling the two configurations, with and without a splice, with 4 antennas in each model yields the preliminary SWR plots in Figures 3.9 and 3.10, respectively. For most applications, an SWR lower than 2 is a good specification for acceptable antenna performance. The two plots have the same relative shape with two minimums around 10.5 MHz and 14 MHz; these two frequencies correspond with SuperDARNs two most commonly used frequencies. The implemented model has a slightly higher SWR at the low end of the range than the ideal model. Also, the implemented model has a lower SWR value at the 10.5 MHz minimum.

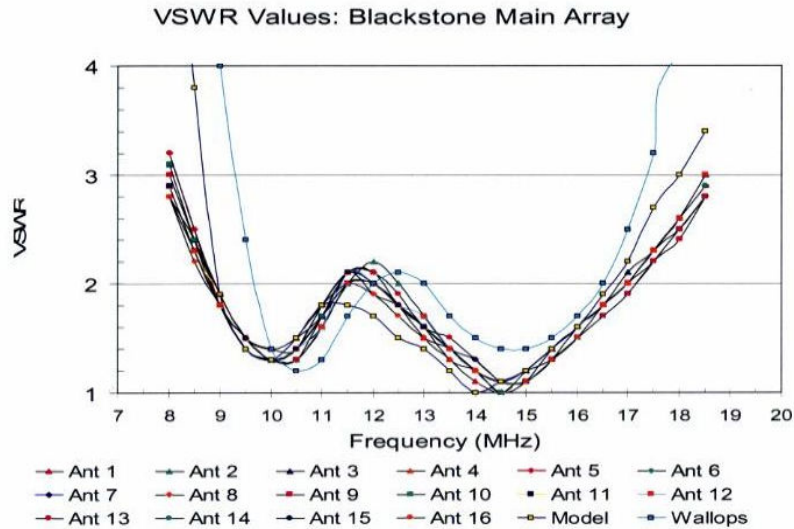


Fig. 3.11 Measured SWR values for individual Blackstone antennas and the average Wallops antenna and for a modified model antenna

The modeled SWR plots seen in Figures 3.9 and 3.10 are similar in shape to SWR measurements taken at Blackstone and Wallops and shown in Figure 3.11. The ideal model shows the same double minima in the SWR as the measurements but does not fluctuate as much as the measurements. The implemented model also slightly shows the double minima in the SWR but does not follow the measurements. The implemented model differs in the fact that the lower frequency minimum has a lower SWR than the higher frequency minimum.

The models presented in Figures 3.9 and 3.10 represent preliminary results from initial understanding about the TTFD antenna. These figures did not exactly match measured results in Figure 3.11 but did give an indication that the models were close to being accurate. Further information about the antenna was gathered during the build of a new radar.

3.5.2. The Hays Learning Experience

In late 2008, SuperDARN collaborators from Virginia Tech, Dartmouth, John Hopkins University, and University of Alaska were awarded a grant from the National Science Foundation to construct eight new radars along middle magnetic latitudes (mid-latitude). These radars would be built in pairs and contribute to the mid-latitude studies already started at the Blackstone and Wallops Island radars. With these ten radars in total, the SuperDARN collaborators intend to study field-aligned irregularities at mid-latitudes during magnetic storms when radars nearer to the poles lose scatter. Construction techniques and challenges for the hardware and antennas associated with the first two of the eight new radars were discussed in Section 2.5. Here, measurements on the TTFD antenna array's characteristics are presented.

<u>SuperDARN Radars</u>			
Location:	<u>Wallops Island, VA</u>	<u>Blackstone, VA</u>	<u>Hays, KS</u>
Year Constructed:	2004-2005	2007-2008	2009
Antenna Pole Height:	50'	56'	56'
Antenna Load:	100 Ohms	75 Ohms	75 Ohms
# of Reflector Wires:	11	21	21
Balun Manufacturer:	SiL	SiL	Array Solutions
Corner Joint:	Through bolt	Butt splice	Butt splice
Frequency Band:	8-18 MHz	8-18 MHz	8-18 MHz

Table 3.2 Local factors impacting antenna array performance

In preparation for the mid-latitude radar chain builds, SuperDARN-Virginia Tech purchased baluns for the 8 radars that were to be built. In a competitive bid, a new supplier, Array Solutions, was chosen after 4 of the sample baluns appeared to meet our specifications as noted in Table 3.2. Of those specifications, the most important one was

a specification for the balun to match a 50 Ohm transmission line to a 1250 Ohm impedance on the antenna side. This specification had been used before with the SiL balun. Due to losses in transformers, the higher impedance side of the balun was thought to be around 1400 to 1500 Ohms.

The Array Solution baluns were field tested when the antennas were put up at the Hays, Kansas radars. By measuring the SWR at the base of the poles, the performance for the Array Solution balun was found to be notably different from what was expected. SWR readings from a few antennas at the Hays radars can be seen in Figure 3.12. The SWR of these antennas sinks to 1.4 at its lowest and goes above 2 within the operating frequencies of the radar.

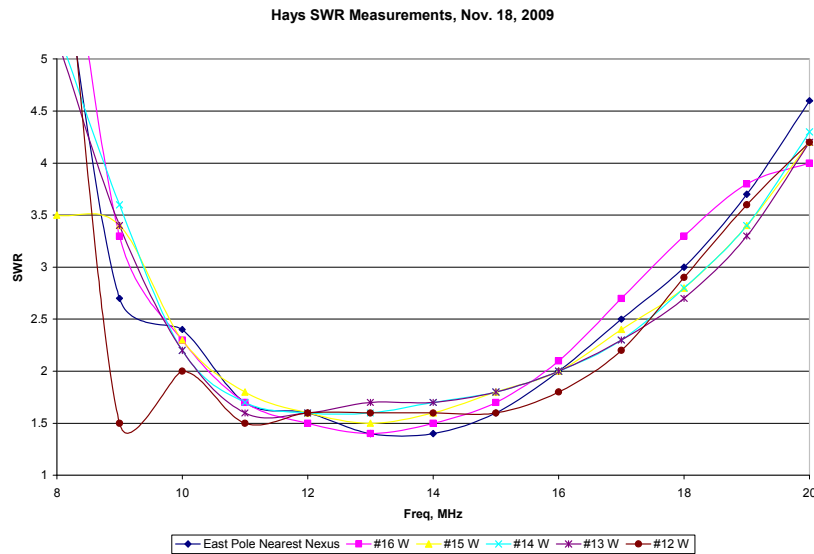


Fig. 3.12 SWR Measurements taken at Hays, KS with the Array Solutions baluns for selected poles

Some thought at the site went into why the SWR readings were so different from readings taken at similar installations at Blackstone and Wallops Island as seen in Figure 3.11, which use SiL baluns. One thought was that the containers for the SiL baluns were

made of metal and the Array Solutions baluns were made of plastic. In theory, with the SiL baluns, the outer conductor of the coaxial cable is connected to the antenna pole since the container of the SiL balun is made of aluminum and is mounted flush against an aluminum plate. A test of this theory at the site with the Array Solution baluns was to connect a short piece of wire from the outer conductor coaxial connector and to connect to a screw which held the balun on to the aluminum plate. This resulted in different SWR readings from what had been seen before originally, but the SWR readings were still not as expected. The resulting SWR readings from the wire modification can be seen in Figure 3.12 on the plot labeled #12 W.

Further thought was put into why the Array Solution baluns performed differently from the SiL balun. Models were developed to try and replicate the balun, additional coaxial cable, and poles such that the model's SWR plot resembled the measured SWR. This model used a wire the approximate diameter of the pole, a 28' piece of transmission line and a 50 Ohm to 1500 Ohm transformer to try to replicate the conditions at the Hays radar. EZNEC does allow for the addition of these objects, but they are ideal and do not account for real world characteristics. The models that included ideal baluns and coaxial cables as well as the poles did not give any clear reason for the unexpected performance of the Array Solution baluns.

Inquiry with Ray Greenwald was made about the plot seen in Figure 3.11 about the line that is labeled 'model'. In looking at this line, and the plots in Figures 3.9 and 3.10, it can be noticed that previous models (Figures 3.9 and 3.10) did not achieve an SWR plot like the 'model' in Figure 3.11. It was then discovered that the model's plot for

Figure 3.11 was generated using a much higher standardizing impedance for the SWR.

The SWR is calculated by:

$$SWR = \frac{1 + |\Gamma|}{1 - |\Gamma|}, \text{ and } \Gamma = \frac{Z_L - Z_0}{Z_L + Z_0}$$

where Γ is the reflection coefficient, Z_L is the antenna input impedance, and Z_0 is the standardizing impedance. Through trial and error it was determined that the standardizing impedance used to generate the plot was somewhere between 2100 and 2400 Ohms. A miscommunication and confusion on the input impedance for the TTFD led for the baluns to be designed to match 50 Ohms to just 1250 Ohms. This difference in the input impedance for the TTFD explained the poor performance of the Array Solutions balun. The impedance mismatch between the antenna side of the balun and the impedance of the TTFD antenna created unwanted reflections and did not transfer all of the energy to the antenna.

An Array Solutions balun was modified systematically and tests were performed by using an impromptu SWR reading setup. This setup involved reading the forward input voltage to the balun as well as reading the reflected voltage through a coupler. The antenna side of the balun was connected to a resistor bridge of several resistors soldered together. The final modification of the balun involved taking 3 turns off of the input side of the balun which increased the transformed impedance on the output side of the balun. The SWR readings from this setup can be seen in Figure 3.13 in which the balun was terminated with roughly 2100 Ohms on the antenna side.

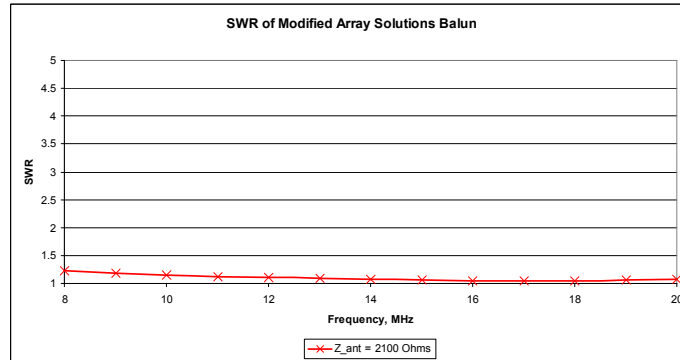


Fig. 3.13 SWR readings from a modified Array Solutions balun terminated into 2100 Ohms on the antenna side.

This modified version of the Array Solutions balun was field tested at the Blackstone radar site. One balun was hung and had SWR readings taken. The modified Array Solutions balun that had three turns taken off the input side did not show good SWR readings which were different than what was expected. After some trial and error, an Array Solutions balun with two turns taken off of the input side seemed to perform best. The SWR readings from this field test of the Array Solutions baluns can be seen in Figure 3.14. As a comparison, SWR readings were taken on an antenna that used an SiL balun and is labeled so in the figure. To get a baseline and try to duplicate the results that were seen at Hays, KS, an unmodified balun was put on an antenna at Blackstone and the SWR measurements were taken. Surprisingly, the SWR measurements on this balun did not match the SWR measurements from Hays as seen in Figure 3.15.

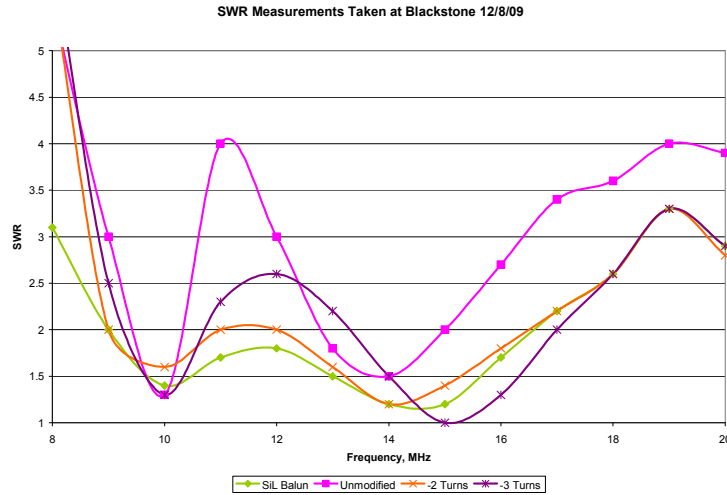


Fig. 3.14 SWR measurements taken at Blackstone in order to field test the modified Array Solutions balun.

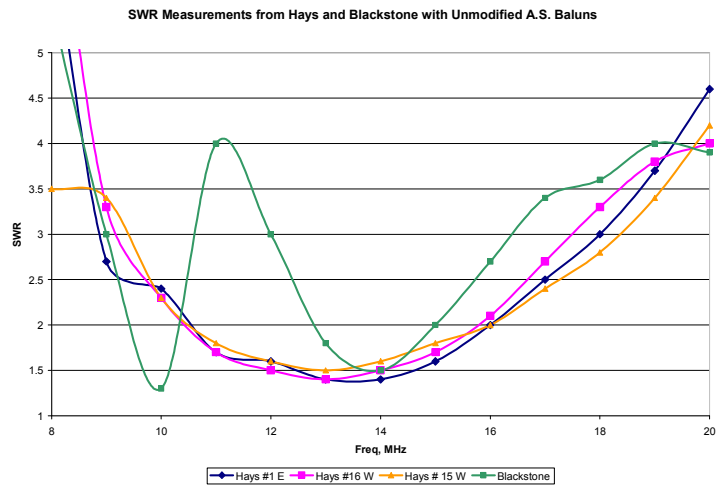


Fig. 3.15 SWR Measurements for similar unmodified baluns mounted on TTFD antennas at Hays and at Blackstone

Regardless of the difference in SWR plots for the unmodified Array Solutions baluns, the modified baluns performed much better than the unmodified balun as seen in Figure 3.14. Even though the -3 Turns plot shows the SWR equal to 1.0 for 15 MHz, the large maximum over 2.0 between 11 and 13 MHz made this balun unacceptable. The -2 Turns balun just barely gets up to an SWR of 2.0. For this reason, the Array Solutions balun that had two turns taken off of the input was chosen to be hung on the 4 antennas

for the interferometer array at Blackstone. Future work is required in order to ensure the correct match for the balun to the TTFD antenna at each radar.

3.5.3. Revisiting the Effect of an Antenna Splice

From the lessons learned during the Hays, KS radar build, the antenna model was updated and corrected. The only thing that needed to be changed was the alternate standardizing impedance that EZNEC uses to calculate the SWR. None of the wire end points were changed and thus the construction of the ideal and implemented antenna designs remained the same.

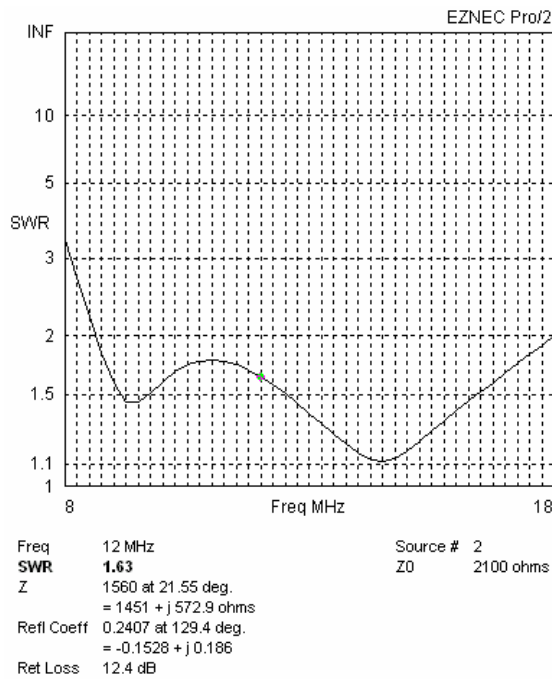


Fig. 3.16 SWR of the ideal antenna model without a splice and with higher standardizing impedance, Z0.

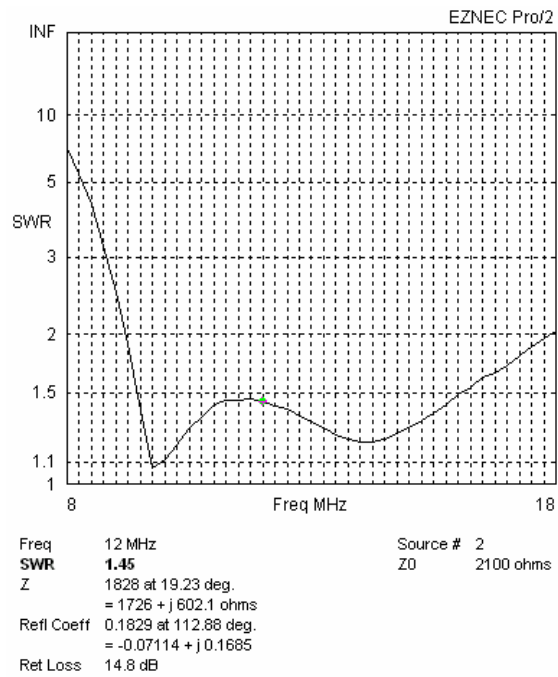


Fig. 3.17 SWR of implemented antenna model with a splice and higher standardizing impedance, Z0.

As can be seen in Figures 3.16 and 3.17, these figures more closely resemble the SWR measurements seen in Figure 3.11 from Blackstone and Wallops than what was originally modeled in Figures 3.9 and 3.10. The higher standardizing impedance, in the plots listed as Z0, yields a higher middle maximum. Also Figure 3.16 matches the

measured SWR values seen in Figure 3.11 since the low frequency minimum has a higher SWR value than the high frequency minimum. Going back to the tests performed earlier which were used to create Figure 3.13, an Array Solutions balun that had two turns removed matched best to a resistor bridge with a resistance of 1800 Ohms. However, Figures 3.16 and 3.17 were created using an antenna impedance of 2100 Ohms which closely resembles the -2 Turns plot in Figure 3.14. Differences between the modeled results and the measured results in Figure 3.11 can be credited to additional effects of real-world losses and loading such as losses through the balun and loading due to the antenna pole.

The modeling of the splice on the TTFD antenna does have an effect on its performance as observed in a SWR plots in Figures 3.16 and 3.17. However through the modeling, no conclusive results can be found to show an accurate model of the splice. Referring back to SWR measurements from Blackstone and Wallops in Figure 3.11, it is noticed that Figure 3.16 resembles measurements at Blackstone which the antenna is built with a splice and Figure 3.17 the model resembles measurements at Wallops which is built without a splice. This result is backwards from what would be expected and further leads to a conclusion that the splice model is not accurate. The discontinuity in Figure 3.17 suggests that an erroneous part introduced with the splice and the NEC2 algorithm cannot resolve the splice, leading to misleading and incorrect results.

3.5.4. Falkland Island Variations

In the process of writing this thesis, the British Antarctic Survey SuperDARN group wanted to move their radar to the Falkland Islands. However, none of the sites identified in the Falkland Islands had a sufficiently level grade along the length required

for the antenna array. The best site had a high point in the middle of the array and slopes down on either side. This radar site planned to use the older Sabre log periodic antennas mentioned earlier. As mentioned before these antennas are built using a heavy tower construction. For the most part, the tops of the concrete pads used to secure the towers into the ground followed the grade of the ground. Also, constructing taller concrete pads to keep the array level can increase costs.

A question was posed to the SuperDARN community on how a sloping antenna array affects the antenna performance. The Falkland Island site was reported to have a grade slope that dropped 2 meters vertically for every 100 meters along the horizontal. Simulating such a ground slope in EZNEC is not straightforward since the program only allows for a horizontal plane at some specified z-coordinate. To try to simulate a sloping ground, a variety of combinations and orientations of an 8-antenna array of log periodic antennas were created. These orientations can be seen in Figure 3.18 which shows how the horizontal axis for each antenna was varied.

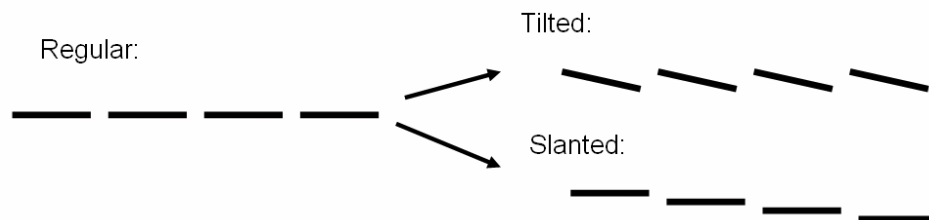


Fig 3.18 Different antenna orientations used to investigate the Falkland Island setup. The bar shows how the horizontal axis for each antenna is manipulated for each variation.

The log-periodic antenna is made of standard tower sections that elevate the log periodic antenna but do not allow the antenna height to be adjustable within a few feet. From the regular half array, a slanted array was created by dropping each antenna down one foot as

the array is extended to eight antennas. For example, the first antenna's center wire had an elevation of 50 feet. The next antenna on the array had the center wire with an elevation of 49 feet. This continued until the last antenna was seven feet below the first antenna. Next, an array was created to resemble the 'tilted' orientation in Figure 3.18. The antenna wires were rotated about the center of the antenna. This rotation is simple in EZNEC since the GUI used for the wire endpoint inputs allows for a user to select a wire or group of wires and rotate the selected wires by a user specified angle and axis. This procedure is then copied down the array until eight antennas are created. Unlike the slanted setup, the antennas were kept at the same elevation in this tilted setup. The orientations and modeling presented replicated several orientations that the log periodic antenna might have in relation to a ground plane.

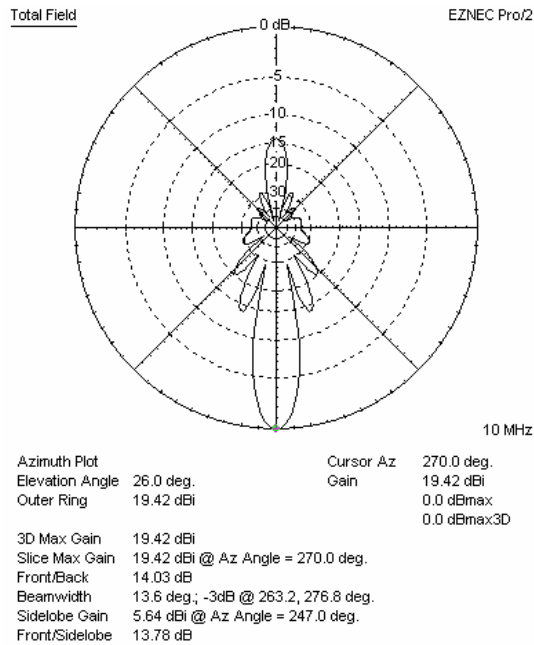


Fig. 3.19 Radiation pattern for 8 log-periodic antennas in a regular orientation

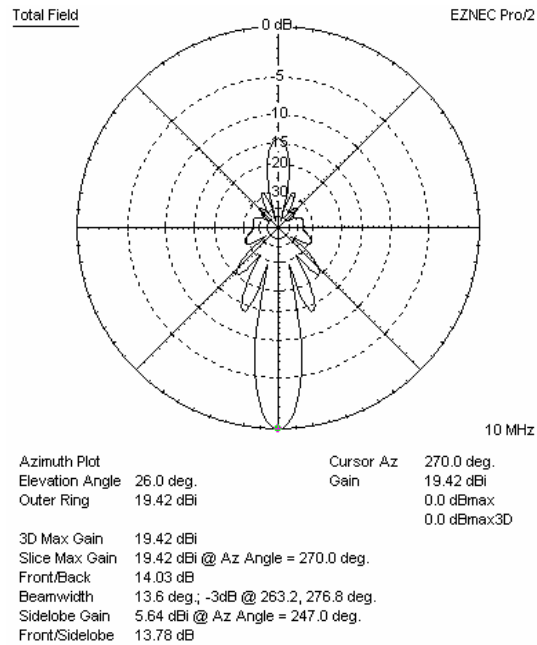


Fig. 3.20 Radiation pattern for 8 log-periodic antennas in a tilted orientation

Each model, including a ‘regular’ model that involved no ground slope or tilting, was simulated with a half array of 8 antennas. This setup followed the Falkland Island situation since plans for the array layout had the ground high point in the middle of the array. Any deviation in the results from the ‘regular’ model is then assumed to double in the full 16 antenna array. However, neither the ‘slanted’ nor the ‘tilted’ models showed a large deviation from the ‘regular’ model in radiation patterns at 10 and 14 MHz. The gains of each model were within a dB of each other and the beamwidth did not vary more than a degree as can be seen in Figures 3.19 and 3.20. As an interesting test of the TTFD design versus the Sabre log-periodic design, the same orientations were repeated for the TTFD antenna array. This test would show if any differences in performance occurred because the TTFD antennas were not level with each other in an array of 8 antennas.

First, all of the TTFD antennas modeled for this section used the ideal antenna model which does not include the splices at the end of the middle horizontal wires. As expected the SWR plot for a middle antenna seen in Figure 3.22 resembles previous modeled and measured SWR plots. The corresponding radiation pattern can be seen in Figure 3.21. As might be expected for a level ground and un-tilted antennas, the pattern is symmetric about the bore sight of the antenna array.

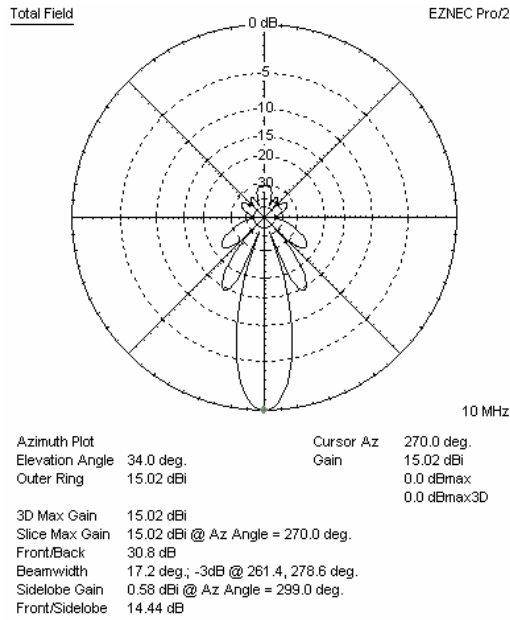


Fig. 3.21 Azimuth plot of radiation pattern for a regular half array of TTFDs

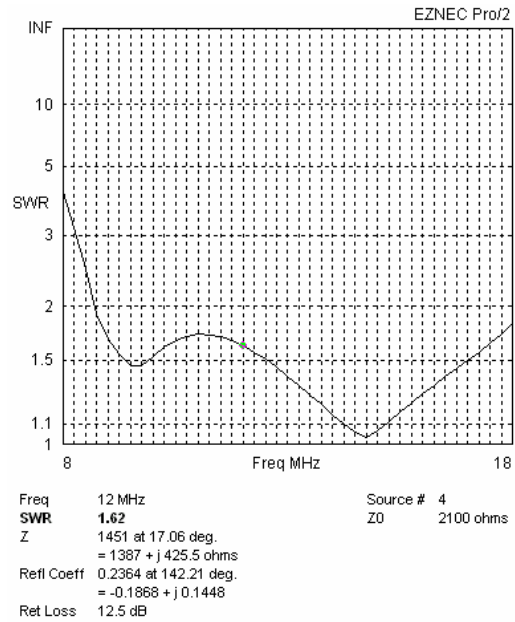


Fig. 3.22 SWR plot for a regular half array of TTFDs

In comparing the patterns for the TTFD antennas in Figure 3.21 and the log-periodic antennas in 3.19, the log-periodic antennas have a better forward gain and narrower beamwidth than the TTFD antenna array. However, the TTFD antenna array has a better front to back ratio than the log-periodic antennas which is an advantage for use with SuperDARN.

For the slanted orientation, the TTFD antenna array used a greater slope by dropping a foot for every 42 feet which is the spacing between TTFD antennas. The corner reflector for the TTFD antenna array was slanted so that the reflector wires were not horizontal. The reflector wires followed that same sloping angle that was used for the TTFD antenna wires. The resulting azimuth radiation pattern at 10 MHz and SWR plot can be seen in Figures 3.23 and 3.24 respectively.

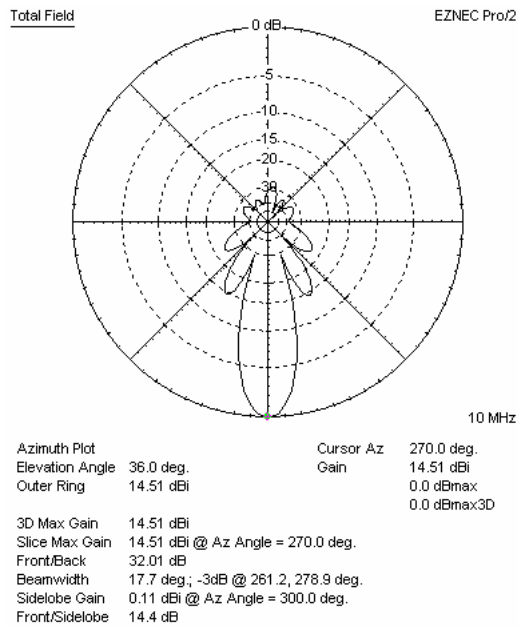


Fig. 3.23 Azimuth plot of radiation pattern for a half array of slanted TTFDs

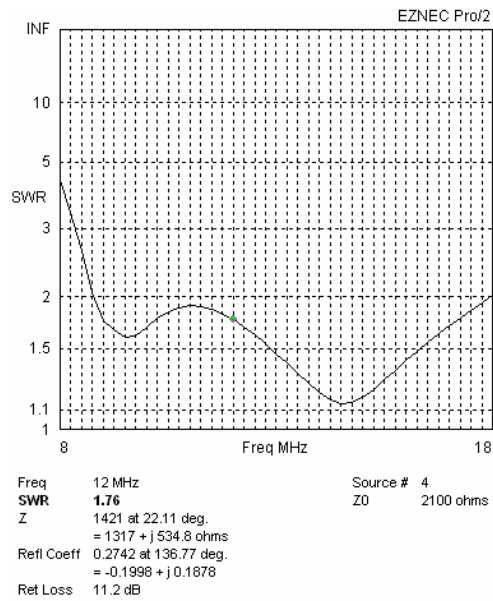


Fig. 3.24 SWR plot for a half array of slanted TTFDs

In looking at the radiation pattern, it can be seen that the pattern is asymmetric mostly in the back part of the pattern. The SWR plot for the slanted array shows some differences from plot for the regular array. In particular, the middle maximum in Figure 3.24 has a higher SWR even though the high frequency minimum crossed the 1.1 line on the plot. The changes in the radiation pattern and the SWR plot are not significant enough to say a slanted array of TTFD antennas is substantially different from a level array.

For the tilted orientation, the six-sided shape of the TTFD antenna was tilted like the tilted orientation in Figure 3.18. However, the corner reflector remained unchanged from the regular half array setup. The resulting azimuth plot and SWR plot for the tilted orientation of the TTFD 8-antenna array can be seen in Figures 3.25 and 3.26 respectively.

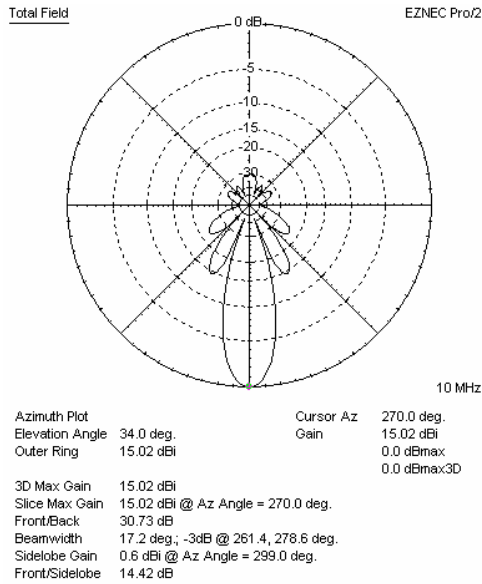


Fig. 3.25 Azimuth plot of radiation pattern for a half array of tilted TTFDs

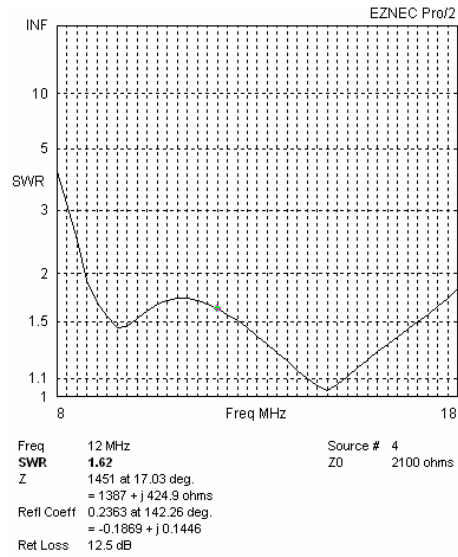


Fig. 3.26 SWR plot for a half array of tilted TTFDs

The azimuth pattern plot in Figure 3.25 appears to be symmetrical about the bore sight of the antenna array even on the backside of the array. Again, the SWR plot for the middle antenna of the tilted TTFD array looks similar to the modeled and measured SWR plots as seen before. However, unlike the slanted array of TTFDs, the SWR values for the middle maximum in Figure 3.26 is lower than the slanted array middle maximum. Also, the SWR values go below 1.1 for the higher frequency minimum. The TTFD antenna array variations in orientation did not show any results in which the antenna array would not work. However, the orientation of the slanted array showed some effects to the antenna array's maximum gain which could affect a radar's performance. Each of the SWR plots for the TTFD antenna orientations did not show any significant problems with SWR. As stated before, EZNEC only deals with horizontal ground planes that can be shifted up or down. However, these ground planes cannot be tilted in order to resemble a grade in the ground. Other modeling software may produce different, more accurate results.



Fig. 3.27 The Falkland Island SuperDARN radar site with newly installed log periodic antennas (Feb. 2010)

The results here were produced by altering the coordinate planes in which the antennas lay by tilting the wires or putting the centers of the antennas on a slope. Ultimately, the results are not surprising given the slope used for the model orientation. A 2 foot drop over 100 feet is not a steep grade and so the array is not significantly changed by this slope. However, it is possible that steeper grades may affect an antenna array's performance.

In reviewing the modeling results for what might be built in the Falkland Islands using the Sabre antennas there did not appear to be any major problems. The results for the Sabre antenna modeling were reported to the British Antarctic Survey group and contributed to a decision to proceed with the build. In the end, the group was able to level the log periodic array with additional height to the concrete pillars as seen in Figure 3.27.

3.5.5. Full Array Modeling

Taking a bit of extra computation time, a full array of TTFD antennas was constructed in the EZNEC program and modeled. This array includes a full 16-antenna array as well as a 4-antenna interferometer array 200' behind the main array. This configuration closely resembles the antenna array layout at Blackstone. One factor at Blackstone that is not taken into account with this model is the lower elevation of the interferometer array. The ground at the Blackstone radar slopes downward toward the back of the array and so the interferometer array is lower than the main array. The interferometer array modeled for the TTFD array for the model is kept level with the main array and is included in this model to show any effects the interferometer array might have on the performance of the main array.

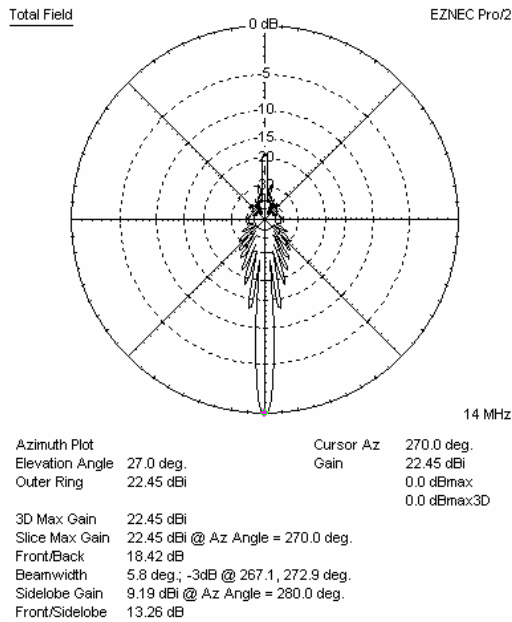


Fig. 3.28 Azimuth pattern at max gain elevation angle for TTFD array at 14 MHz

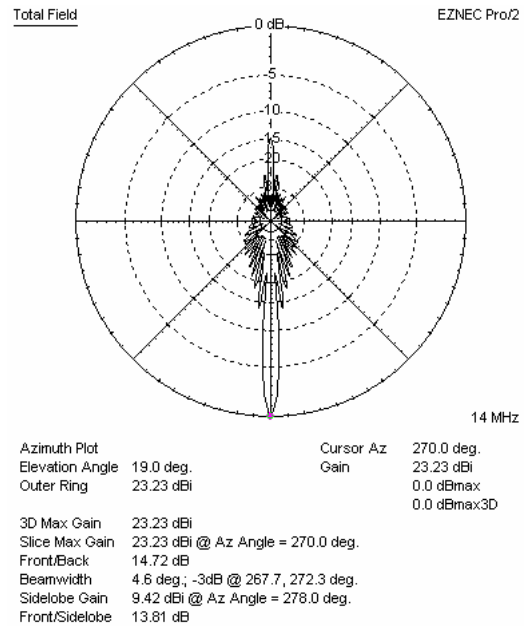


Fig. 3.29 Azimuth pattern at max gain elevation angle for log-periodic array at 14 MHz

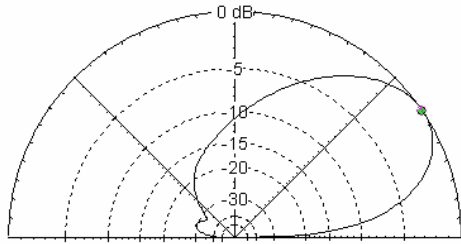
Figure 3.28 shows the horizontal radiation pattern at 14 MHz for the full TTFD antenna array. As expected with more antennas, the number of sidelobes has increased

from previous 4- and 8-antenna models. Also in this figure, the narrow beamwidth desired for radars is shown with a calculated beamwidth of 6° . This model was also run at 10 MHz and the back lobe is much less at 10 MHz than it is at 14 MHz. The front-to-back ratio for 10 MHz is calculated as 32.75 dB and for 14 MHz is calculated as 18.42 dB. This difference may be due to the shorter wavelength at 14 MHz and the corner reflector allowing more of the energy to pass through to the back of the array.

As a comparison to the previously used log-periodic design, the result for a full array of log-periodic antennas with an interferometer array is presented in Figure 3.29. The TTFD antenna array lacks a few decibels of gain and has a wider beamwidth by a couple of degrees in comparison to the log periodic array. However, the TTFD antenna array model shows a higher front-to-back ratio for both frequencies modeled. This ratio is important for high latitude radars since stronger unwanted signals can appear if the back lobe of the antenna array is too strong.

To complete the analysis of the full array of TTFD antennas, the elevation patterns for the array at 10 and 14 MHz are presented in Figures 3.30 and 3.31. The differences between the two figures show the variation of the radiation pattern with frequency for the TTFD antenna. Also, the significantly lower back lobe can be observed in Figure 3.30. The large beamwidth noted in both of these figures for the elevation angle shows that the TTFD antenna allows for signals to be transmitted and received from several angles of elevation. This characteristic is important for the antenna's use with SuperDARN since the desired take-off angle varies depending on conditions of the ionosphere.

Total Field EZNEC Pro/2

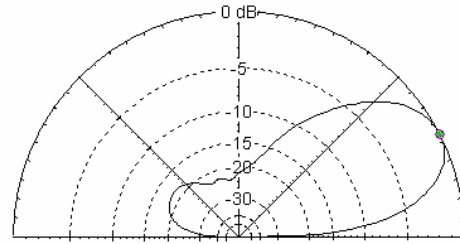


10 MHz

Elevation Plot		Cursor Elev	34.0 deg.
Azimuth Angle	270.0 deg.	Gain	18.96 dBi
Outer Ring	18.96 dBi		0.0 dBmax
			0.0 dBmax3D
3D Max Gain	18.96 dBi		
Slice Max Gain	18.96 dBi @ Elev Angle = 34.0 deg.		
Beamwidth	41.9 deg., -3dB @ 16.1, 58.0 deg.		
Sidelobe Gain	-10.51 dBi @ Elev Angle = 162.0 deg.		
Front/Sidelobe	29.47 dB		

Fig. 3.30 The elevation pattern of an array of TTFD antennas at 10 MHz

Total Field EZNEC Pro/2



14 MHz

Elevation Plot		Cursor Elev	27.0 deg.
Azimuth Angle	270.0 deg.	Gain	22.46 dBi
Outer Ring	22.46 dBi		0.0 dBmax
			0.0 dBmax3D
3D Max Gain	22.46 dBi		
Slice Max Gain	22.46 dBi @ Elev Angle = 27.0 deg.		
Beamwidth	32.7 deg., -3dB @ 12.7, 45.4 deg.		
Sidelobe Gain	4.35 dBi @ Elev Angle = 145.0 deg.		
Front/Sidelobe	18.11 dB		

Fig. 3.31 The elevation pattern of an array of TTFD antennas at 14 MHz

Both the log periodic and TTFD antenna arrays are used as phased array systems in which the furthest off boresight that the radar scans is about 29 degrees. Even for off-boresight beams, the same differences in patterns between the log-periodic and the TTFD antenna apply. Azimuth patterns for two different frequencies for a steered beam of the TTFD antenna array are presented in Figures 3.32 and 3.33 in which the grating lobe is clearly visible in Figure 3.33. Important to note about these figures, EZNEC calculates the front-to-back ratio by using the gain in the main lobe for the ‘front’ and using the pattern gain 180° in azimuth from the main lobe for the ‘back’. Figure 3.33 shows the pattern for the TTFD antenna array at 18 MHz which is the upper limit of the radar’s operating frequency. Also, Figures 3.32 and 3.33 show the main beam to be steered further than the stated 29 degrees because of over-steering of the beam through the use of modified phasing. This over-steering effect is currently used at the Wallops and Blackstone radars and allows the radar to have a larger field-of-view.

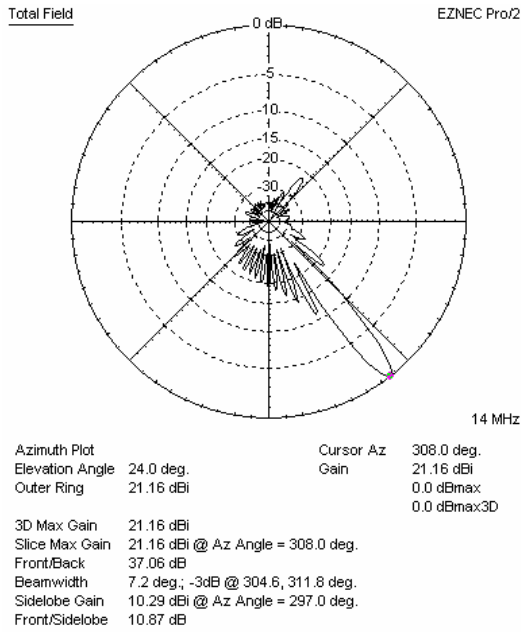


Fig. 3.32 Azimuth pattern of a full TTFD array steered to one extreme of the array's scan at 14 MHz

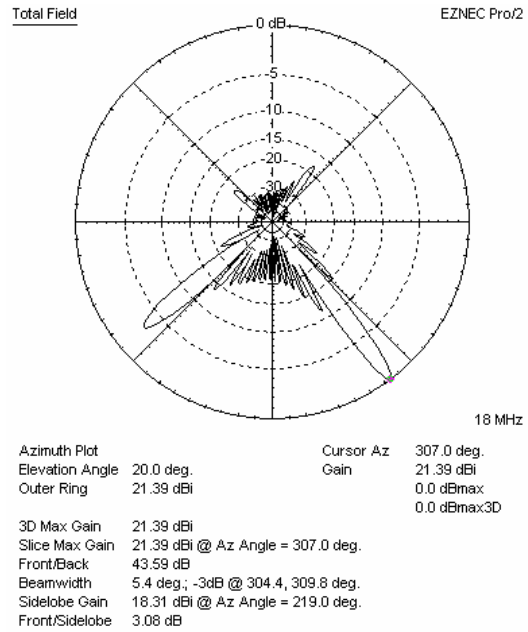


Fig. 3.33 Azimuth pattern of a full TTFD array steered to one extreme of the array's scan at 18 MHz

The primary results of the earlier modeling of a prototype TTFD antenna in respect to directionality and front-to-back ratio are confirmed with the modeling of the full array. This high ratio for the TTFD antenna is an advantage for radars operating at high latitudes where returns and noise from the back-lobe can be a problem. An array of TTFD antennas delivers acceptable performance with the stated frequency range of the SuperDARN radar and is a suitable replacement to the log-periodic antenna array.

4. Conclusions and Future Work

The SuperDARN group continues to expand its radar coverage and its knowledge of field-aligned plasma irregularities. SuperDARN will be adding six additional radars which will follow the site constructed in 2009 in Hays, Kansas as a model. These additional radars will be built in pairs at locations in the areas of Oregon and the far Aleutian Islands in the United States and a final pair located in the Azores. The design strengths and flaws of the antenna array as well as the techniques and challenges of constructing the antenna array presented here will provide useful information for these future builds as the design of the radar system will be consistent for each site.

The analysis of the transmit and receive paths of the University of Leicester electronics will provide future SuperDARN members insight into the design of the radar from a system level. Analysis of the receiver front end installed at the Kapuskasing site will serve as important documentation and insight for a standard SuperDARN front end receiver. The development of the transmitter test unit provides a simple solution for testing the functionality of a transmitter by simulating radar operation characteristics.

The modeling results of the TTFD antenna array using EZNEC, which is based on the NEC2 algorithm, show that this new antenna design provides a radiation pattern with a narrow beamwidth which is required for radar antennas. Variations on this design are

shown to minimally affect the overall performance of the antenna array which provides for a bit more flexibility in constructing a TTFD antenna array. As noted in the Hays experience with the TTFD antennas, the input impedance for the TTFD antenna is higher than originally expected. A balun should be specified to match 50 Ohms to 1800 Ohms in order to have an effective match over the operating range.

The modeling results also show slight differences when a splice is introduced to the TTFD model. The NEC2 algorithm may not be the best way to accurately account for effects introduced with the splice. The short wire created in the splice model comes close to violating requirements for the thin wire approximation, used in NEC2, to not introduce errors in the final solution. These short wires have a length to wire radius ratio of around 10 to 15 and for the solution to have less than 1% error because of the thin wire approximation, this ratio must be greater than 8. Also, these short wires do not allow for several segments to be created on each wire since each wire length is already much shorter than the 2 to 3 foot segment length used in this model. One segment for each of these wires will not allow for the current expansion functions to properly create currents along the short section of wire.

For the first time a model for a full array of TTFD antennas is compared to a full array of log-periodic antennas. From the results of the full array modeling, it is observed that the TTFD antenna array provides for a higher front-to-back ratio than the log-periodic antenna. This ratio is particularly important for antennas used at SuperDARN sites at high latitudes since radar returns from the back lobe of the antenna can produce false results.

Other antenna modeling packages may better represent and compute the effects on the TTFD antenna's performance. One of these other modeling packages is FEKO, which could also be used to study the effects of an uneven ground on the TTFD antenna array's performance. To completely understand the TTFD antenna array's performance and measure its characteristics, the radiation pattern needs to be measured. For most antennas, this measurement is performed in an anechoic chamber in which a known signal source radiates electromagnetic energy towards the test antenna. The radiation pattern is gathered by measuring the received power level and rotating the test antenna. This measurement cannot be done with a TTFD antenna array since the antenna is about 800' long in its longest dimension. Very few anechoic chambers of that size exist and the ones that do are outside of the resources of SuperDARN and Virginia Tech. A solution to this measurement is to take the idea of the anechoic chamber and reverse the roles of the test antenna and the known signal source. This type measurement has been performed once before for a prototype TTFD antenna. Future work on the radiation pattern measurement of a TTFD antenna array may follow the previous measurement that is described in Appendix C.

Appendix A: Wire Endpoints for Single TTFD in EZNEC for the Ideal Model

<u>Wire No.</u>	<u>End 1 Coord. (ft)</u>			<u>End 2 Coord. (ft)</u>			<u>Dia (in)</u>	<u>Segments</u>	<u>Insulation</u>	
	<u>X</u>	<u>Y</u>	<u>Z</u>	<u>X</u>	<u>Y</u>	<u>Z</u>			<u>Diel C</u>	<u>Thickness (in)</u>
1	-42	0	58	42	0	58	0.080808	25	1	0
2	-42	2	56	42	2	56	0.080808	25	1	0
3	-42	4	54	42	4	54	0.080808	25	1	0
4	-42	6	52	42	6	52	0.080808	25	1	0
5	-42	8	50	42	8	50	0.080808	25	1	0
6	-42	10	48	42	10	48	0.080808	25	1	0
7	-42	12	46	42	12	46	0.080808	25	1	0
8	-42	14	44	42	14	44	0.080808	25	1	0
9	-42	16	42	42	16	42	0.080808	25	1	0
10	-42	18	40	42	18	40	0.080808	25	1	0
11	-42	20	38	42	20	38	0.080808	25	1	0
12	-42	22	36	42	22	36	0.080808	25	1	0
13	-42	24	34	42	24	34	0.080808	25	1	0
14	-42	24	30	42	24	30	0.080808	25	1	0
15	-42	22	28	42	22	28	0.080808	25	1	0
16	-42	20	26	42	20	26	0.080808	25	1	0
17	-42	18	24	42	18	24	0.080808	25	1	0
18	-42	16	22	42	16	22	0.080808	25	1	0
19	-42	14	20	42	14	20	0.080808	25	1	0
20	-42	12	18	42	12	18	0.080808	25	1	0
21	-42	10	16	42	10	16	0.080808	25	1	0
22	-18	0	32	18	0	32	0.080808	11	1	0
23	18	0	32	13	0	36	0.080808	3	1	0
24	13	0	36	-13	0	36	0.080808	9	1	0
25	-13	0	36	-18	0	32	0.080808	3	1	0
26	-18	0	32	-13	0	28	0.080808	3	1	0
27	-13	0	28	13	0	28	0.080808	9	1	0
28	13	0	28	18	0	32	0.080808	3	1	0

Appendix B: Wire Endpoints for Single TTFD in EZNEC for the Implemented Model

<u>Wire No.</u>	<u>End 1 Coord. (ft)</u>			<u>End 2 Coord. (ft)</u>			<u>Dia (in)</u>	<u>Segments</u>	<u>Insulation</u>	
	<u>X</u>	<u>Y</u>	<u>Z</u>	<u>X</u>	<u>Y</u>	<u>Z</u>			<u>Diel C</u>	<u>Thickness (in)</u>
1	-42	0	58	168	0	58	0.0808	25	1	0
2	-42	2	56	168	2	56	0.0808	25	1	0
3	-42	4	54	168	4	54	0.0808	25	1	0
4	-42	6	52	168	6	52	0.0808	25	1	0
5	-42	8	50	168	8	50	0.0808	25	1	0
6	-42	10	48	168	10	48	0.0808	25	1	0
7	-42	12	46	168	12	46	0.0808	25	1	0
8	-42	14	44	168	14	44	0.0808	25	1	0
9	-42	16	42	168	16	42	0.0808	25	1	0
10	-42	18	40	168	18	40	0.0808	25	1	0
11	-42	20	38	168	20	38	0.0808	25	1	0
12	-42	22	36	168	22	36	0.0808	25	1	0
13	-42	24	34	168	24	34	0.0808	25	1	0
14	-42	24	30	168	24	30	0.0808	25	1	0
15	-42	22	28	168	22	28	0.0808	25	1	0
16	-42	20	26	168	20	26	0.0808	25	1	0
17	-42	18	24	168	18	24	0.0808	25	1	0
18	-42	16	22	168	16	22	0.0808	25	1	0
19	-42	14	20	168	14	20	0.0808	25	1	0
20	-42	12	18	168	12	18	0.0808	25	1	0
21	-42	10	16	168	10	16	0.0808	25	1	0
22	-17.5	0	32	17.5	0	32	0.0808	11	1	0
23	17.5	0	32	17.5	0	32.04	0.0808	1	1	0
24	17.5	0	32	17.5	0	31.96	0.0808	1	1	0
25	17.5	0	32.04	17.75	0	32.04	0.0808	1	1	0
26	17.5	0	31.96	17.75	0	31.96	0.0808	1	1	0
27	17.75	0	32.04	12	0	36	0.0808	3	1	0
28	12	0	36	-12	0	36	0.0808	9	1	0
29	-12	0	36	-17.75	0	32.04	0.0808	3	1	0
30	-17.75	0	31.96	-12	0	28	0.0808	3	1	0
31	-12	0	28	12	0	28	0.0808	9	1	0
32	12	0	28	17.75	0	31.96	0.0808	3	1	0
33	-17.5	0	32	-17.5	0	32.04	0.0808	1	1	0
34	-17.5	0	32	-17.5	0	31.96	0.0808	1	1	0
35	-17.5	0	32.04	-17.75	0	32.04	0.0808	1	1	0
36	-17.5	0	31.96	-17.75	0	31.96	0.0808	1	1	0

Appendix C: Results of a Previous Measurement of a TTFD Antenna

A TTFD antenna was constructed next to the Saskatchewan SuperDARN radar using five vertical poles or small towers. The construction plans for the radiating wires is shown in Figure C.1. Instead of using Teflon cable to support the radiating wires, a combination of rope and fiberglass tubing creates the structure of the TTFD shape. The five-wire reflector was constructed using two towers and running the conducting wire horizontally between the towers. The simulated radiation pattern can be verified by taking measurements of signal strength around the antenna.

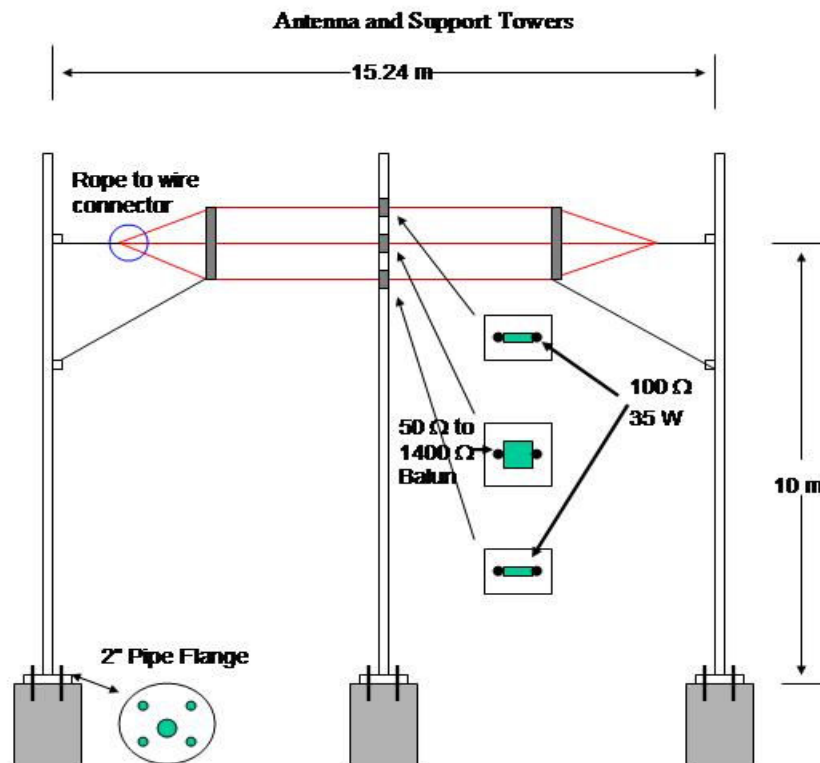


Fig. C.1 TTFD construction at Saskatoon [20]

In order to measure the pattern of the antenna in three dimensions, measurements must be taken at several heights above the level of the antenna. The best way to perform a three dimensional measurement in the far field of the antenna is to use an airplane to fly around the antenna. To make the measurement automated and eliminate human error, a laptop using a logging program was connected to a GPS unit and an A/D converter which processed AGC voltage from a receiver. The TTFD antenna was excited by a signal coming from a signal generator and passed through an amplifier. The signal was received on an 8 meter long wire which was dragged behind the airplane. In order to ensure the wire trailed straight behind the plane, a funnel was tied to the end of the wire to act as a drag. The measurement setup can be seen in block diagram form in Figure C.2. Every two seconds the GPS unit sent the location of the airplane to the laptop. Simultaneously, the A/D converter digitized the AGC voltage coming from the receiver. These two signals were logged in the laptop and saved for later analysis.

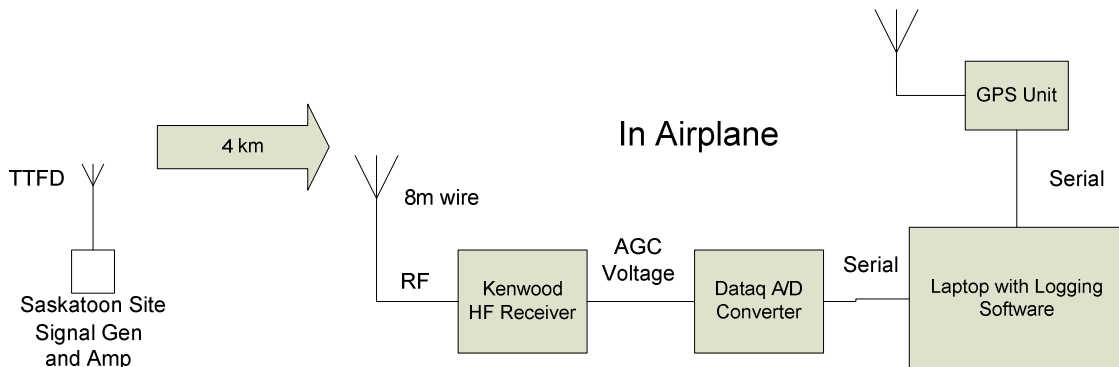


Fig. C.2 Measurement Setup performed at Saskatoon

The airplane flew in a circle of a radius of 4 kilometers in order to ensure the measuring antenna was in the far-field of the prototype TTFD antenna. This distance was also chosen so that the airplane was able to fly to altitudes in which an elevation angle of

30° can be measured. The flight was setup so that the elevation pattern was measured between 10° and 30° in 5° intervals. However, due to changes in the flight plan because of a nearby airport and failure of the laptop battery not all the desired measurements were taken.

Once back on the ground, the measurements were converted to decibels and corrected for changes in distance from the prototype TTFD antenna to the measurement antenna. This correction would ensure that the path loss was constant among all the measurements since the plane could not fly at a constant distance from the antenna. These results were then interpolated to yield useful data in 1° intervals of elevation angle between 13° and 21° at 14 MHz and between 19° and 21° at 10 MHz. Figure C.3 shows the azimuth radiation pattern plots for different elevation angles for 14 MHz. Between each dotted contour is 5 dB.

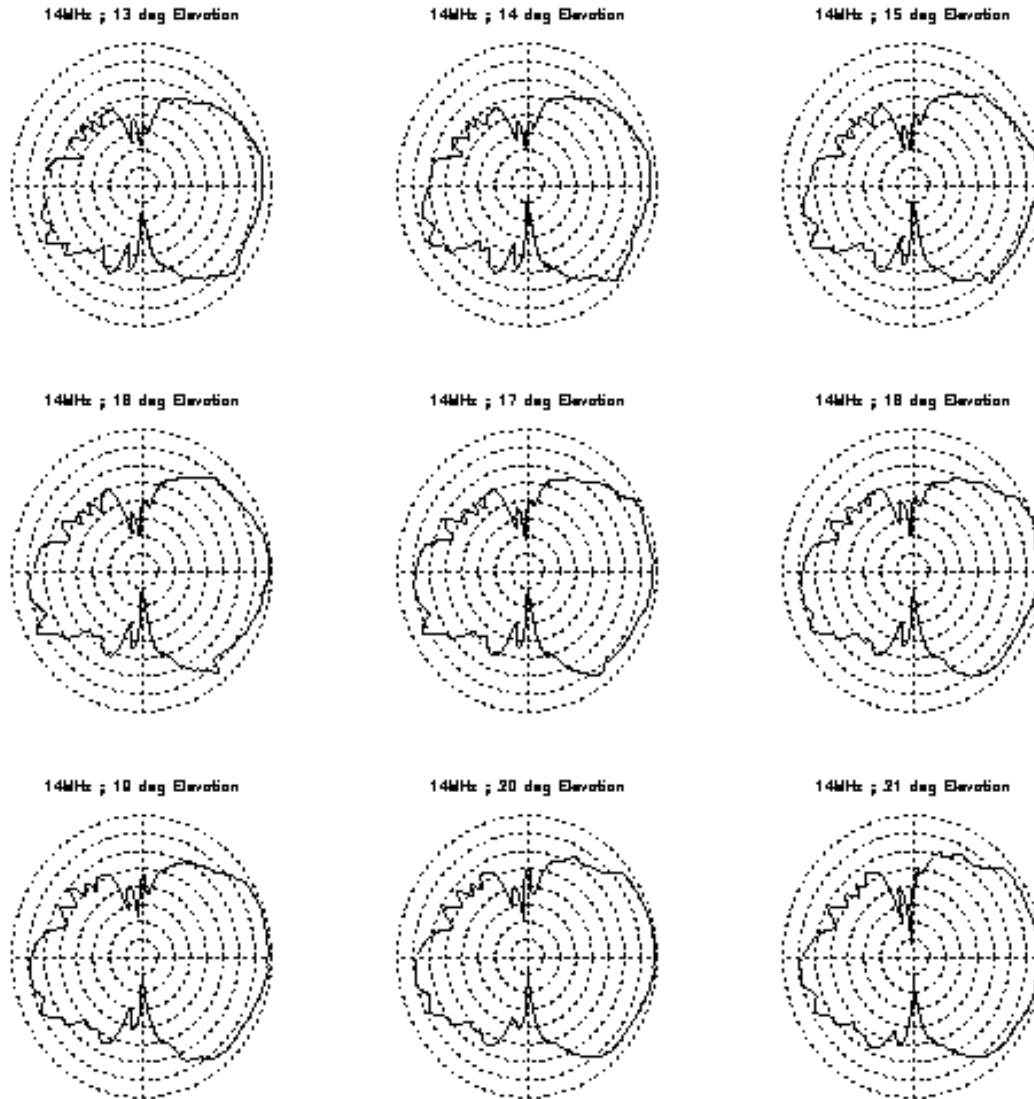


Fig. C.3 Radiation pattern plots from the measurements taken at Saskatoon of the prototype TTFD antenna with the dashed lines representing 5dB [20]

The pattern plots were similar to the pattern plots from the model of the antenna in EZNEC. The measured front-to-back ratio, 5-10 dB, was not similar to the ratio given by the model, about 13.5 dB, and the shape of the plot was slightly different. The measured pattern showed an asymmetry of the back lobe. In testing at Saskatoon, the TTFD antenna had been built next to the existing interferometer array which consisted of log-periodic antennas. The energy radiated by the TTFD coupled into these antennas and

made the measured pattern asymmetric. Further modeling of the log-periodic antennas next to the TTFD antenna accounted for this asymmetry. From this analysis, the TTFD antenna was deemed a suitable replacement for the Sabre antenna design.

List of References

- [1] Breit, G., Tuve, M. A., *A Test of the Existence of the Conducting Layer*, Phys. Rev., Vol. 28, p. 554, 1926
- [2] University of Leicester, Svalbard Ionosonde, <http://ion.le.ac.uk/ionosonde/cadi/experiment.html>
- [3] Ionograms, GOLF website, <http://www.golfp.com/ionograms/index.php>
- [4] Abel, W. G., Edwards, L.C., *The source of long distance backscatter*, Proceedings IRE, Vol. 39, pp. 1538- 1541, 1951.
- [5] Bates, H. F., *Direct HF backscatter from F-region*, J. Geophys Res, Vol. 65, pp. 933-2002, July, 1960.
- [6] Gordon, W. E., *Incoherent scattering of radio waves by free electrons with applications to space exploration by radar*, Proceedings IRE, Vol. 46, p. 1824-1829, 1958.
- [7] Bowles, K. L., *Observations of vertical incidence scatter from the ionosphere at 41 Mcps*, Physics Review Letters, Vol. 1, p. 454-455, December, 1958.
- [8] Ecklund, W. L., Balsley, B. B., Greenwald, R. A., *Crossed beam measurements of the diffuse radar aurora*, Journal of Geophysical Research, Volume 80, Number 13, pp 1805-1809, May 1975.
- [9] Greenwald, R. A., Weiss, W., Nielsen, E., Thomson, N. R., *STARE: A new radar auroral backscatter experiment in northern Scandinavia*, Radio Science, Volume 13, Number 6, pp 1021-1039, Nov-Dec 1978.
- [10] Greenwald, R. A., Baker, K. B., Villain, J. P., *Initial studies of small-scale F region irregularities at very high latitudes*, Radio Science special issue on radio probing of the high latitude ionosphere and atmosphere, Vol. 18, p. 1122-1132, Nov. 1983.
- [11] Greenwald, R. A., Baker, K. B., Hutchins, R. A., Haniuse, C., *An HF phased-array radar for studying small-scale structure in the high-latitude ionosphere*, Radio Science, Vol. 20, No. 1, p. 63-79, January 1985.

- [12] Greenwald, R. A., Baker, K. B., Ruohoniemi, J. M., *Experimental Evaluation of the propagation of high-frequency radar signals in a moderately disturbed high-latitude ionosphere*, Johns Hopkins APL Technical Digest, Vol. 9, No. 2, 1988.
- [13] Greenwald, R. A., et al., *DARN/SUPERDARN, A Global View of the Dynamics of High Latitude Convection*, Space Science Review, 71, pp. 761-796, 1995.
- [14] Chisham, G., et al., *A decade of the Super Dual Auroral Radar Network (SuperDARN): scientific achievements, new techniques and future directions*, Surveys in Geophysics, Vol. 28, pp. 33-109, 2007.
- [15] Ruohoniemi, J. M., Baker, K. B., *Large-scale imaging of high-latitude convection with Super Dual Auroral Radar Network HF radar observations*, J. Geophys. Res., Vol. 103, No. 20, p. 797, 1998.
- [16] <http://superdarn.jhuapl.edu/rt/map/index.html>, SuperDARN JHU-APL website.
- [17] Baker, J. B. H., Ruohoniemi, J. M., Shepard, S. G., McWilliams, K. A., Greenwald, R. A., Bristow, W. A., *Those DARN Radars: New Directions for the Super Dual Auroral Radar Network*, Proceedings of Union Radio-Scientifique Internationale, 2008.
- [18] Online. Available: <http://www.bwantennas.com/ama/amaindex.htm>
- [19] Kraus J. D., Marhefka, R. J., *Antennas for all applications*, McGraw-Hill, New York, 2002.
- [20] André, D., Greenwald, R. A., Marshall, W., *A new antenna for SuperDARN radars; Design, Implementation and Verification*, Unpublished Manuscript.
- [21] Burke, G. J.; Poggio, A. J., *Numerical Electromagnetics Code (NEC) – Method of Moments, Program Description – Theory*, 1981, Lawrence Livermore Laboratory, Available: <http://www.nec2.org>.
- [22] Poggio, A. J., Adams, R. W., *Approximations for Terms Related to the Kernel in Thin-Wire Integral Equations*, UCRL-51985, Lawrence Livermore Laboratory, CA, December 19, 1975.
- [23] Harrington, R. F., *Field Computation by Moment Methods*, MacMillan, New York, 1968.
- [24] Yeh, Y. S. and Mei, K. K., *Theory of Conical Equiangular Spiral Antennas, Part I – Numerical Techniques*, IEEE Trans. Antennas and Propagation, AP-15, 1967, p. 634.

- [25] Sommerfeld, A., *Partial Differential Equations in Physics*, Academic Press, New York, 1964.
- [26] Norton, K. A., *The Propagation of Radio Waves Over the Surface of the Earth and in the Upper Atmosphere*, Proceedings of the Institute of Radio Engineers, Vol. 26, No. 9, Sept. 1937.
- [27] Rubin, D., *The Linville Method of High Frequency Transistor Amplifier Design*, Naval Weapons Center, Research Department, NWCCL TP 845, Corona Laboratories, Corona California, March 1969.